UNCLASSIFIED

SECURITY CLASSIFICATION OF THIS PAGE *(When Data Entered)*

REPORT DOCUMENTATION PAGE

READ INSTRUCTIONS BEFORE COMPLETING FORM

1. REPORT NUMBER

2. GOVT ACCESSION NO.

3. RECIPIENT'S CATALOG NUMBER

4. TITLE *(and Subtitle)*
Locking of Diode Gain Modules Using Optical Conjugation Techniques

5. TYPE OF REPORT & PERIOD COVERED
FINAL REPORT
1 Aug 1982 - 30 Sept 1983

6. PERFORMING ORG. REPORT NUMBER

7. AUTHOR(s)
J.F. Lam and D.A. Rockwell

8. CONTRACT OR GRANT NUMBER(s)
N00014-82-C-0535

9. PERFORMING ORGANIZATION NAME AND ADDRESS
Optical Physics Department
Hughes Research Laboratories
Malibu, CA 90265

10. PROGRAM ELEMENT, PROJECT, TASK AREA & WORK UNIT NUMBERS

11. CONTROLLING OFFICE NAME AND ADDRESS
Office of Naval Research, Dept. of the Navy
800 N. Quincy St.
Arlington, VA 22217

12. REPORT DATE
March 1984

13. NUMBER OF PAGES
82

14. MONITORING AGENCY NAME & ADDRESS*(if different from Controlling Office)*

15. SECURITY CLASS. *(of this report)*
Unclassified

15a. DECLASSIFICATION/DOWNGRADING SCHEDULE

16. DISTRIBUTION STATEMENT *(of this Report)*

Approved for public release; distribution unlimited.

17. DISTRIBUTION STATEMENT *(of the abstract entered in Block 20, if different from Report)*

18. SUPPLEMENTARY NOTES

19. KEY WORDS *(Continue on reverse side if necessary and identify by block number)*

Diode lasers
Semiconductor lasers
Laser power scaling
Phase conjugate resonator

20. ABSTRACT *(Continue on reverse side if necessary and identify by block number)*

This report reviews results of a study program to investigate technical issues relating to the coupling of multiple diode lasers using a phase conjugate resonator. We present calculations showing the effects on the far-field intensity distribution of either systematic or random phase differences between adjacent gain elements; these results dramatically illustrate the beneficial impact of exact phase locking.

DD FORM 1 JAN 73 1473 EDITION OF 1 NOV 65 IS OBSOLETE

UNCLASSIFIED

SECURITY CLASSIFICATION OF THIS PAGE *(When Data Entered)*

The use of phase conjugation to phase-lock the individual emitters is suggested, and computer calculations showing the beneficial effects on the far-field intensity distribution are reviewed. The normal modes of a multiple-element diode chip are derived; this information allows one to determine phase relationships characteristic of each mode. These relationships can be used to identify approaches that might be employed to favor one particular mode in a practical device. Calculations have been completed showing that a phase conjugate mirror based on stimulated Brillouin scattering (SBS) in either a CS_2-filled hollow light pipe, or a solid fused silica waveguide is possible in this spectral range at power levels of only $\lesssim$ 1 watt. The advantage of the SBS phase conjugate mirror is that no external pumps are required, leading to an improved overall system efficiency. Because potential applications involve nonlinear optical devices, we address issues related to achieving efficient nonlinear wavelength conversion with a diode-based source. Thermal problems in a high average power frequency doubler can be minimized using beam shaping; this technology is reviewed. Previous experimental demonstrations have established the feasibility of frequency-doubling the output of diode lasers and have indicated the relevant scaling laws. Using this information, we estimate that an extracavity doubling efficiency of 40 percent is possible using thirteen commercial GaAlAs diodes with non-critically phase matched $KNbO_3$.

LOCKING OF DIODE GAIN MODULES USING OPTICAL CONJUGATION TECHNIQUES

J.F. Lam and D.A. Rockwell

Hughes Research Laboratories
3011 Malibu Canyon Road
Malibu, CA 90265

March 1984

N00014–82–C–0535
Final Report
1 August 1982 through 30 September 1983

OFFICE OF NAVAL RESEARCH
Department of the Navy
800 N. Quincy Street
Arlington, VA 22217

TABLE OF CONTENTS

LIST OF ILLUSTRATIONS

LIST OF ILLUSTRATIONS (CONTINUED)

LIST OF ILLUSTRATIONS (CONTINUED)

LIST OF ILLUSTRATIONS (CONTINUED)

FOREWORD

This final report describes the 14-month investigation on U.S. Navy contract N00014-82-C-0535. The study was performed by the Optical Physics Department, Hughes Research Laboratories, Malibu, California 90265. Dr. David A. Rockwell was the program manager, and Dr. Juan F. Lam was the principal investigator. The authors acknowledge Dr. H.W. Yen of the Optical Circuits Department for his enthusiastic technical support in areas related to diode laser device physics. Other contributions came from Drs. R.L. Abrams, W.B. Brown, R.C. Lind, T.R. O'Meara, and G.C. Valley. The technical expertise of C.L. Slayman is also acknowledged.

Work performed on this program was administered by the Office of Naval Research, Arlington, Virginia. Dr. H. Pilloff was the ONR Project Scientist.

SECTION 1

INTRODUCTION

This report presents the results of a study program to investigate concepts for coherent coupling of multiple GaAlAs diode gain elements to produce a laser system with the potential for generating high average output power. It is desired that the resulting laser source have sufficient brightness to ensure efficient nonlinear wavelength conversion, such as frequency-doubling into the blue-green spectral region.

The concept of combining multiple gain modules into a single coherent output beam has traditionally been approached by techniques such as injection locking, diffraction coupling, or a combination of these. By constrast, this report assumes a new approach to phase-locking modular gain media utilizing the technology area of nonlinear optical phase conjugation. To understand how optical phase conjugation techniques can be used for this purpose, consider a resonator structure which employs a phase conjugate mirror (PCM) as one element of the cavity. Such a structure is known as a phase conjugate resonator (PCR). Figure 1 shows a PCR structure applied to locking three gain media. A generic PCR has phase and frequency properties that are substantially different from a conventional resonator. First, the output phase profile is relatively insensitive to aberrations within the gain medium.[1-4] In a conventional resonator even small internal aberrations cause large diffractive losses and greatly degrade the output beam. Second, since we are considering PCRs that use four-wave mixing conjugators, the output frequency is controlled by the conjugator pumps. Stripped of details, the four-wave mixer conjugator, through the action of pumps 1 and 2, couples the phase and frequency of the gain modules to that of the pumps. The phase at the output coupling mirror becomes uniform and results in a far-field radiation pattern possessing a central lobe and a specific side-lobe level as in any thinned array.

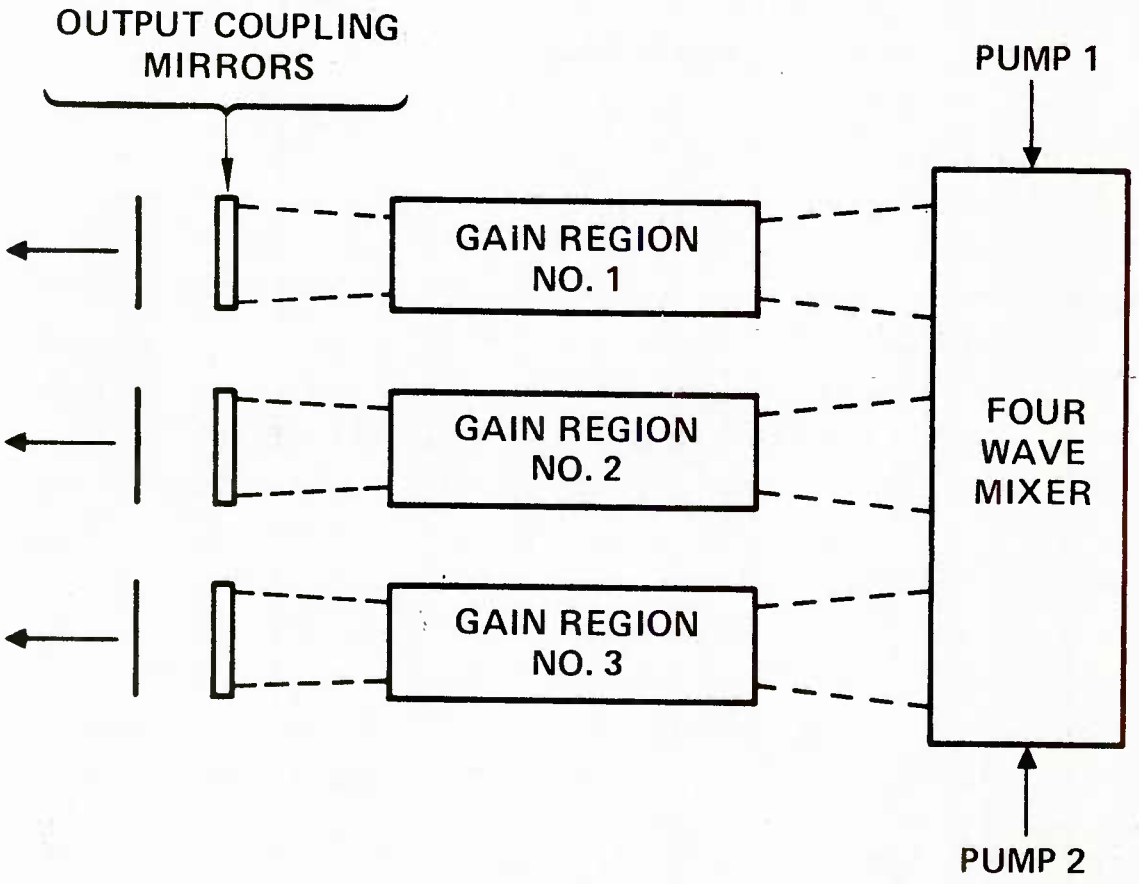

Figure 1. Generic PCR structure applied to coupling modular lasers by four-wave mixing.

The actual experimental demonstration of such a concept is beyond the scope of the present program. Instead, effort has been directed toward several specific technical areas related to coupling multiple diode gain elements, as well as some specific issues relating to achieving phase conjugation and efficient nonlinear wavelength conversion within the 800-900 nm spectral range accessible to GaAlAs laser devices. To enhance the ultimate applicability of this program to systems applications, it has been implicitly assumed that many diode gain elements are fabricated on a single, practical, monolithic chip. Chip size or the total number of chips could, in principle, be scaled according to the system power requirement. Section 2 presents calculations showing the effects on the far-field intensity distribution of either systematic or random phase differences between adjacent gain elements; these results dramatically illustrate the beneficial impact of exact phase locking. Next, the use of phase conjugation to phase-lock the individual emitters is presented. Computer calculations showing the beneficial effects on the far-field intensity distribution are reviewed. Next, the normal modes of a multiple-element diode chip are derived. This information allows one to determine phase relationships characteristic of each mode. These relationships can be used to identify approaches that might be employed to favor one particular mode in a practical device. Section 3 presents calculations showing that a phase conjugate mirror based on stimulated Brillouin scattering (SBS) in either a CS_2-filled hollow light pipe, or a solid fused silica waveguide is possible in this spectral range at power levels of only $\lesssim$ 1 watt. The advantage of the SBS phase conjugate mirror is that no external pumps are required, leading to an improved overall system efficiency. Section 4 addresses issues relating to achieving efficient nonlinear wavelength conversion with a diode-based source, and presents an approach for minimizing thermal problems in a high average power frequency doubler. Previous experimental

demonstrations have established the feasibility of frequency-doubling the output of diode lasers and have indicated the relevant scaling laws. Using this information, we estimate that an extracavity doubling efficiency of 40 percent is possible using thirteen commerical GaAlAs diodes with non-critically phase matched $KNbO_3$. This assumes that the beam compacting problem has been solved.

SECTION 2

COUPLED GAIN MEDIA

Many techniques have been suggested for combining multiple gain elements into a single coherent beam. These techniques include injection locking and path synchronization, diffraction coupling, and combinations of these. Figure 2 illustrates two systems that use injection locking to couple multiple elements. Figure 3 shows a schematic of diffraction coupling with a reflective spatial filter. In general, injection locking of multiple diode elements appears unattractive because of the requirement that the effective path length of each element (the product of the refractive index and the geometric length) must be controlled to within a small fraction of a wavelength. Diffraction coupling has been investigated by others [5,6] and is not the subject of the current program. Recently, phase conjugate reflection by four-wave-mixing has developed to the point where it may be used to build a multiple gain-module laser with phase and frequency locking. Figure 1 showed a system with a four-wave-mixing conjugator used to couple the modules. The analysis presented in this section was undertaken to provide a framework within which coupling techniques can be compared and evaluated. We begin with a discussion of the far-field intensity distribution that arises by coupling multiple gain elements, and show the degradation in the far-field intensity distribution that arises from uncompensated phase differences between individual emitters. The next section illustrates how phase conjugation compensates such phase differences to improve beam quality. Far-field effects arising from physical gaps between emitters (to allow for heat sinks, for example) are presented next, along with some basic approaches to minimize these deleterious effects. We conclude with a calculation of the normal modes of a multiple planar waveguide, representing the multi-element diode chip assumed to be the basic building block of these diode coupling concepts.

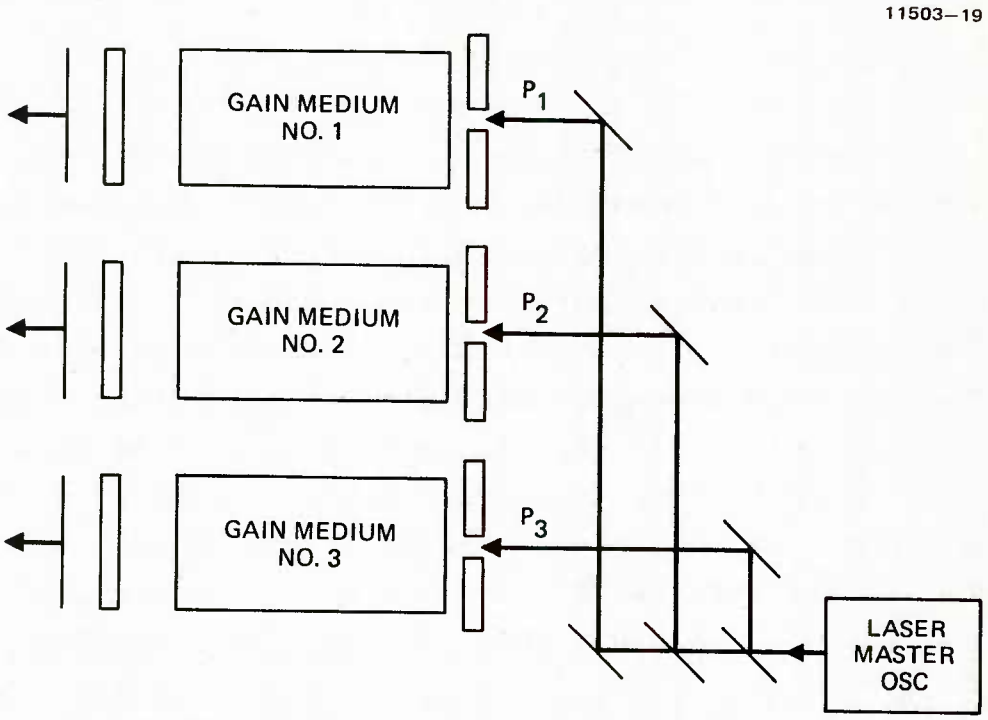

a. INJECTION LOCKING TO A COMMON MASTER OSC

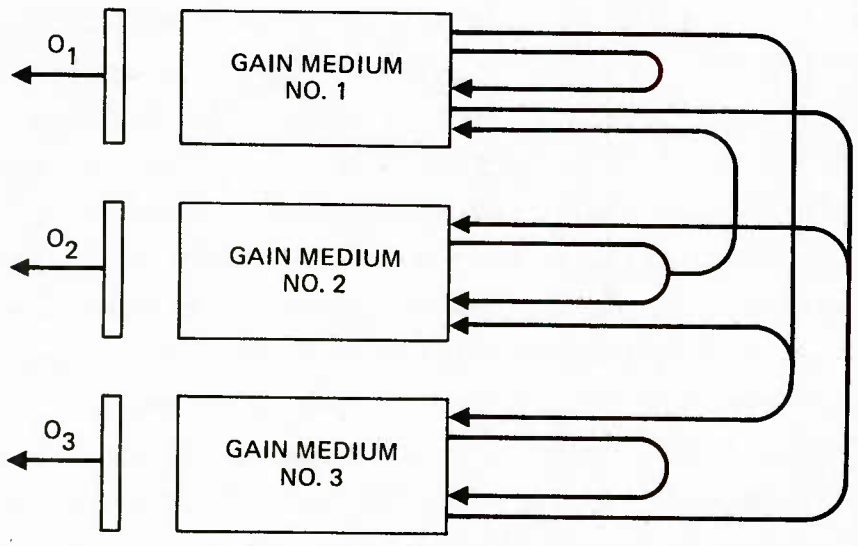

b. INJECTION LOCKING VIA MUTUAL COUPLING.
THE CROSS COUPLING ILLUSTRATED HERE IS SCHEMATIC

Figure 2. Two classes of injection locking techniques. Neither of these techniques ensures a co-phased output for wavefronts O_1, O_2, and O_3.

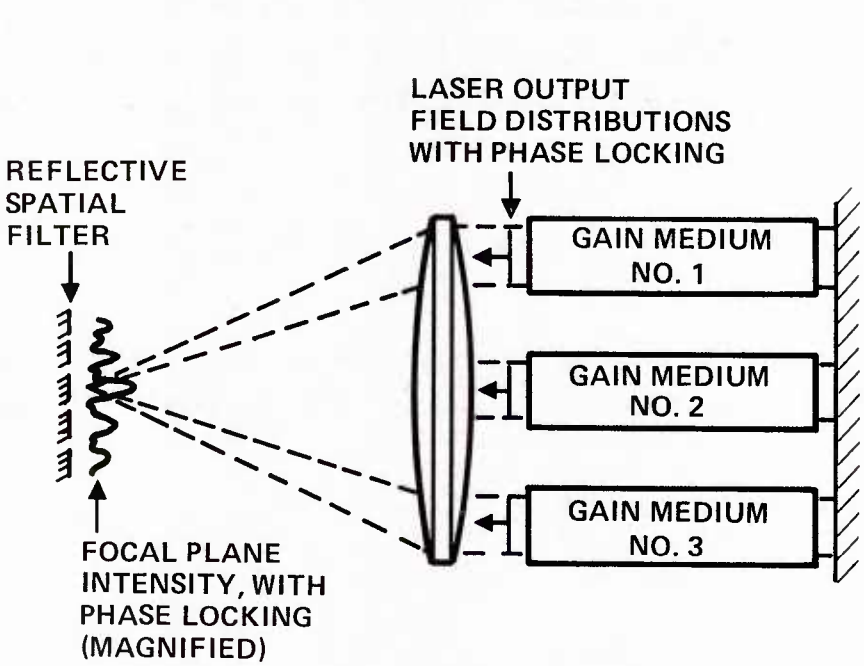

Figure 3. Phase-locking of three lasers by diffraction coupling with spatial filters.

2.1 FAR-FIELD INTENSITY DISTRIBUTION OF A PHASED LASER ARRAY

The understanding of a phased laser array entails the knowledge of the relative phases between adjacent lasers. In general, it is a quite complicated problem due to the uncertainty in the semiconductor laser parameters, i.e., current density, index of refraction, gain homogeneity, etc. However, it is possible to estimate the magnitude of the phase shifts by examining the changes arising from temperature variation, doping concentration and gain length. The optical phase ϕ is defined as

$$\phi = \frac{2\pi}{\lambda_o} nL \tag{1}$$

where λ_o is the vacuum wavelength, n is the index of refraction and L is the propagation distance. The change in ϕ is then

$$\Delta\phi = \frac{2\pi}{\lambda_o} \{\Delta n L + n\Delta L\} \tag{2}$$

or,

$$\Delta\phi = \frac{2\pi}{\lambda_o} \{[(\Delta n)_t + (\Delta n)_c] L + n\Delta L\} \tag{3}$$

where $(\Delta n)_t$ and $(\Delta n)_c$ are the contributions due to the temperature and dopant concentration respectively. In a semiconductor laser, the contribution to Δn due to a temperature change is estimated[7] to be $dn/dT = 3 \times 10^{-4}/°K$ at 850 nm. Hence for a temperature change of 20°C, the change in the index of refraction amounts to approximately 6×10^{-3}. The contribution due to fluctuations in the dopant concentration is estimated[8] to be 10^{-2} for a concentration of the order of 10^{18} cm^{-3} at 900 nm. If a diode laser array is produced in a single crystal, then cleavage along a crystal plane yields a typical error[9] in the crystal length of the order of $\Delta L = 3$ μm. If one assumes that

the index of refraction of the gain medium is 3.6., the gain length is 300 μm, and the wavelength is 850 nm, Eq. (3) yields

$$\Delta\phi = 1.1 \times 10^2 \text{ rad.} \tag{4}$$

which is a significant phase change between the individual lasers.

It is appropriate to determine the effects of such phase shifts on the far-field intensity distribution or, equivalently, the distribution of the focused output of a phased laser array. In view of recent experimental demonstrations[10-12] of diffraction-coupled GaAs diode lasers, we examine the problem by assuming a set of emitters having certain specific phase relations. These studies lead to an understanding of the experimental demonstrations.

The geometry under consideration is shown in Figure 4. The intensity distribution at the focal spot f is given by[13]

$$I(x,y) = \frac{1}{\lambda^2 f^2} \left| \int_{-\infty}^{\infty} dx' \int_{-\infty}^{\infty} dy' \, \mathcal{E}(x',y') \, e^{-i\frac{2\pi}{\lambda f}(xx' + yy')} \right|^2 \tag{5}$$

in the Fresnel limit, where $\mathcal{E}(x',y')$ is the input field to the lens, i.e., it is the electric field distribution of the emitters. We assume for simplicity that the array is 1-Dimensional, along the x-axis, and the electric field is an identical Gaussian for all emitters. Hence the electric field for the n^{th} emitter is

$$\mathcal{E}_n(x) = \mathcal{E}_o e^{-\frac{(x-x_n)^2}{2a_o^2}} e^{i\phi(x_n)} \tag{6}$$

where a_o is the spot size and x_n is the position of the n^{th} laser. $\phi(x_n)$ is the phase of the n^{th} laser. The evaluation of the intensity distribution using Eq. (6) is straightforward, and the results are now presented for different sets of phase shift parameters.

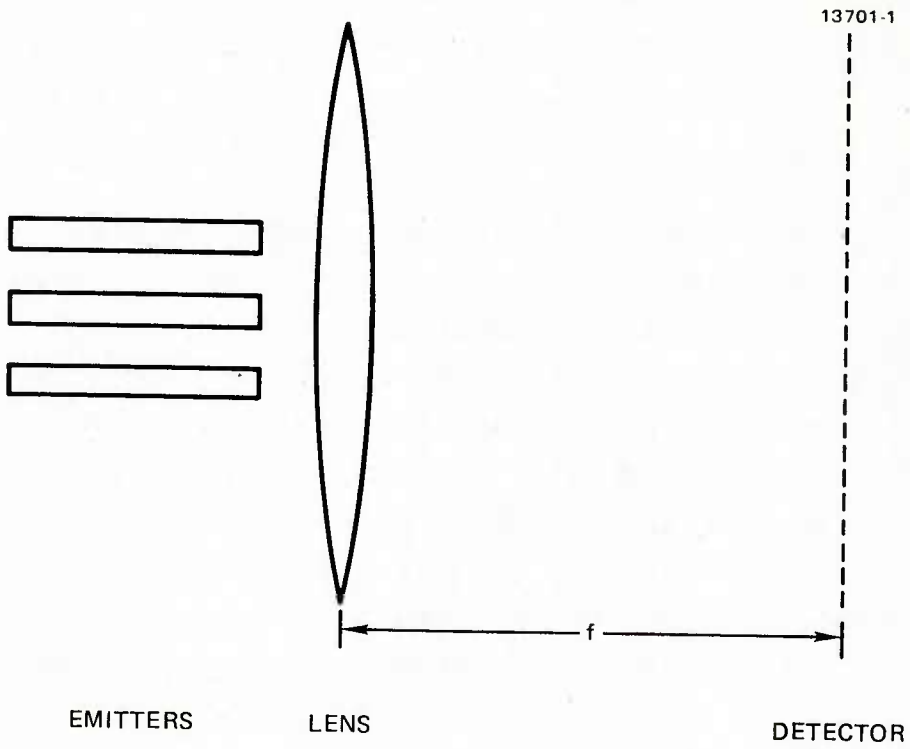

Figure 4. Geometry for the calculation of the focused output of an array of emitters.

The first case to be considered is shown in Figure 5 where we assume two emitters are in phase with each other. The results to be shown have the separation between lasers normalized to the focal spot, i.e., the normalization constant is $a_e = \lambda f/2\pi a_o$. a_o is taken to be 3 μm. Figure 6 represents the focused intensity when the separation between the emitters is 5 μm. As the separation increases to 10 μm, one observes that additional side lobes appear as shown in Figure 7. This behavior arises from simple diffraction and interference of the electromagnetic waves. The existence of the central lobe in the output intensity is an intrinsic property of the in-phase assumption.

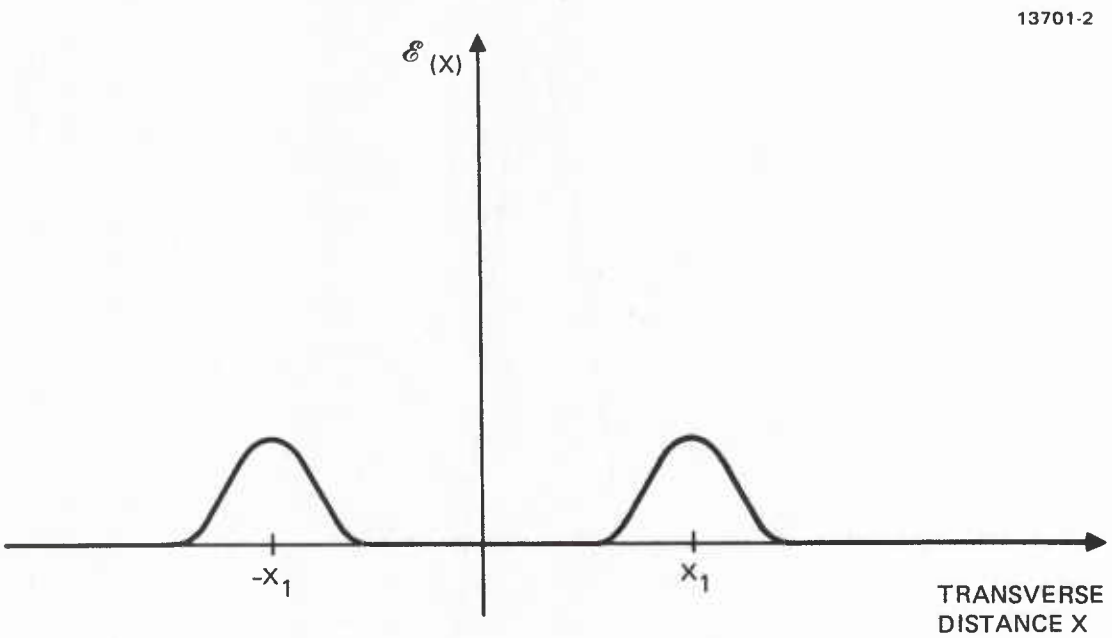

Figure 5. Input field distribution for two in-phase emitters.

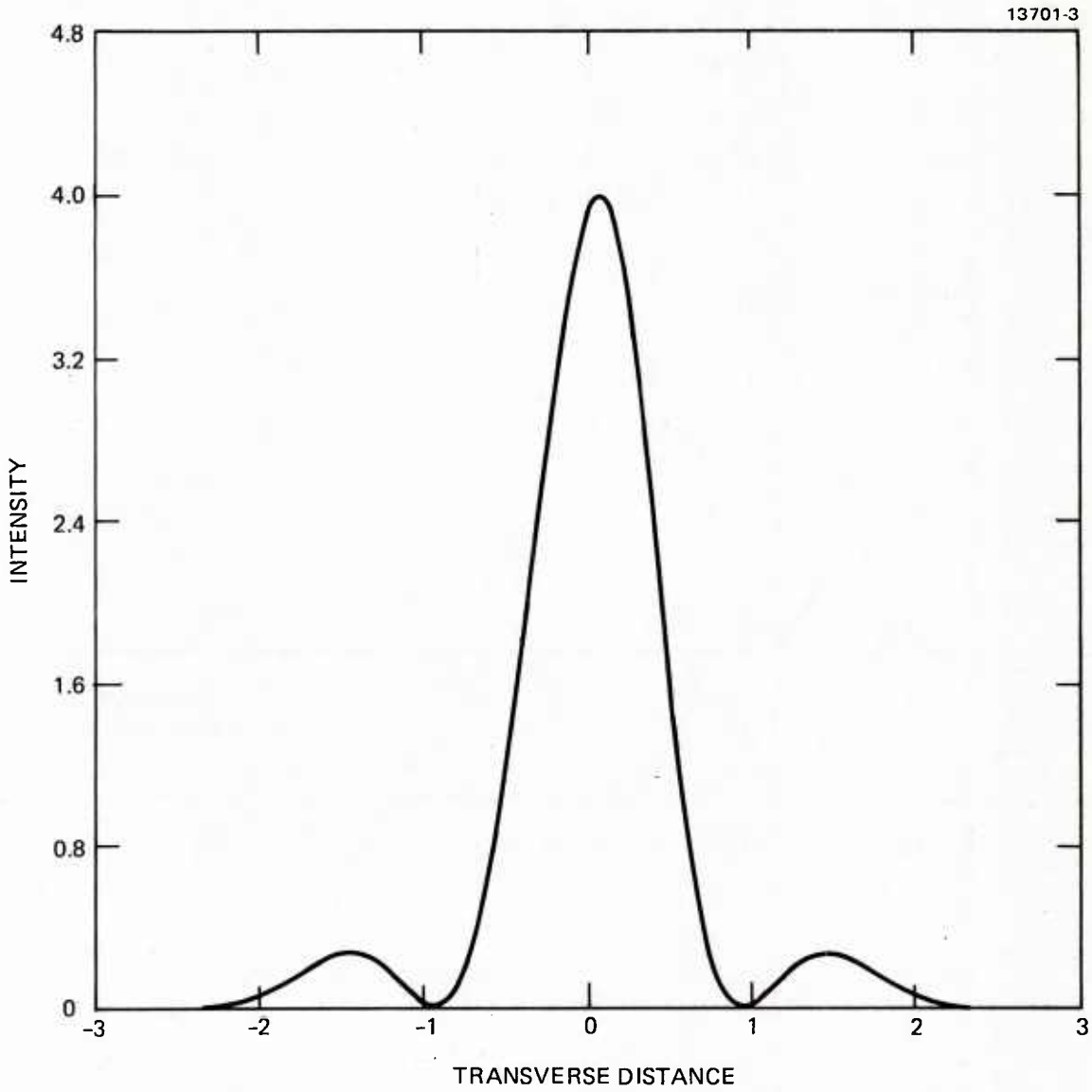

Figure 6. Output intensity for the in-phase case where the separation between emitters is 5 μm. Transverse distance is measured in units of $(\lambda f/2\pi a_o)$.

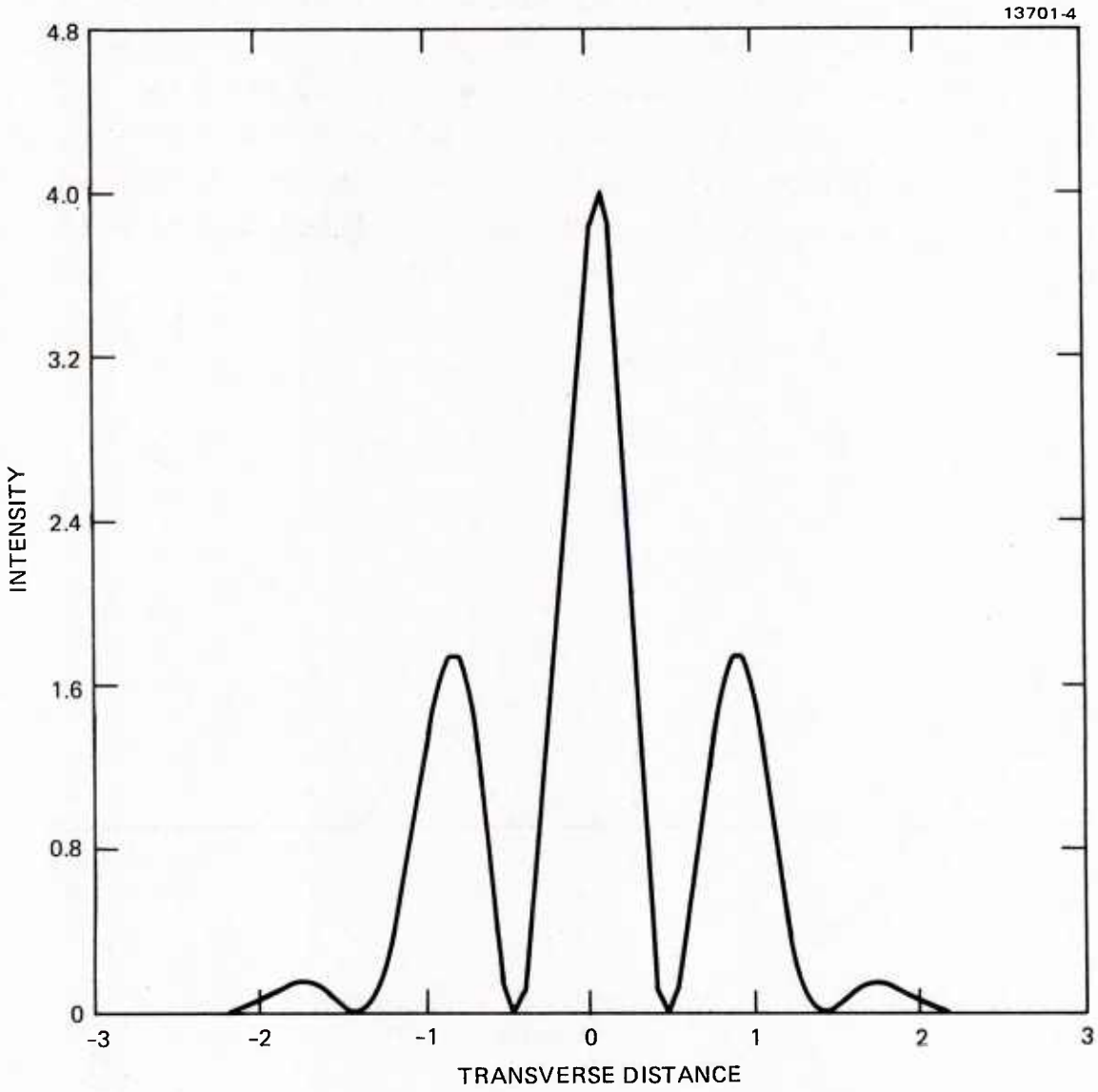

Figure 7. Output intensity for the in-phase case where the separation between emitter is 10 μm. Transverse distance is measured in units of $(\lambda f/2\pi a_o)$.

In contrast to the in-phase situation, Figure 8 considers the case of two emitters which are 180° out of phase. The focused output intensity distribution is shown in Figure 9 for the case where the separation between the emitters is 5 μm. The absence of the central lobe (in comparison to the in-phase case) is due to the destructive interference of the two electromagnetic waves which are 180° out of phase with respect to each other. Increasing the separation of 10 μm yields additional side lobes due to diffraction effects.

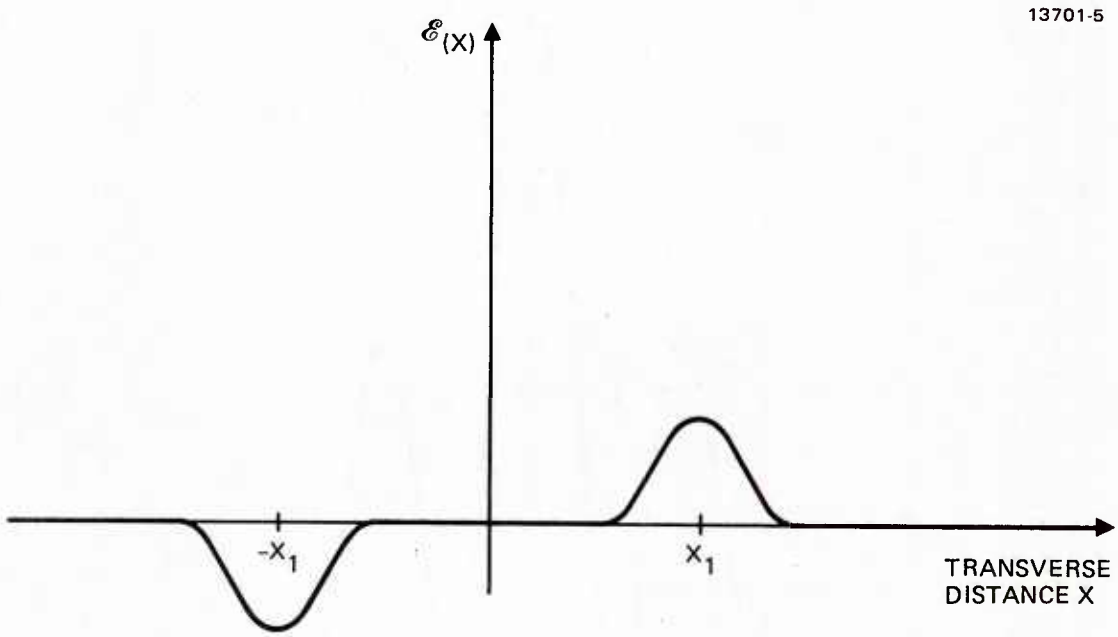

Figure 8. Input field distribution for two 180° out-of-phase emitters.

Next, we consider cases representative of the experiments reported in the literature.[10-12] We assume 10 emitters, each having a spot size of the order of 3 μm. Figure 10 illustrates the input field distribution. First we shall consider the case where all emitters are in-phase. The output intensity distributions are shown in Figures 11 and 12. Again, the central lobe is very apparent in both figures and is due to the constructive nature

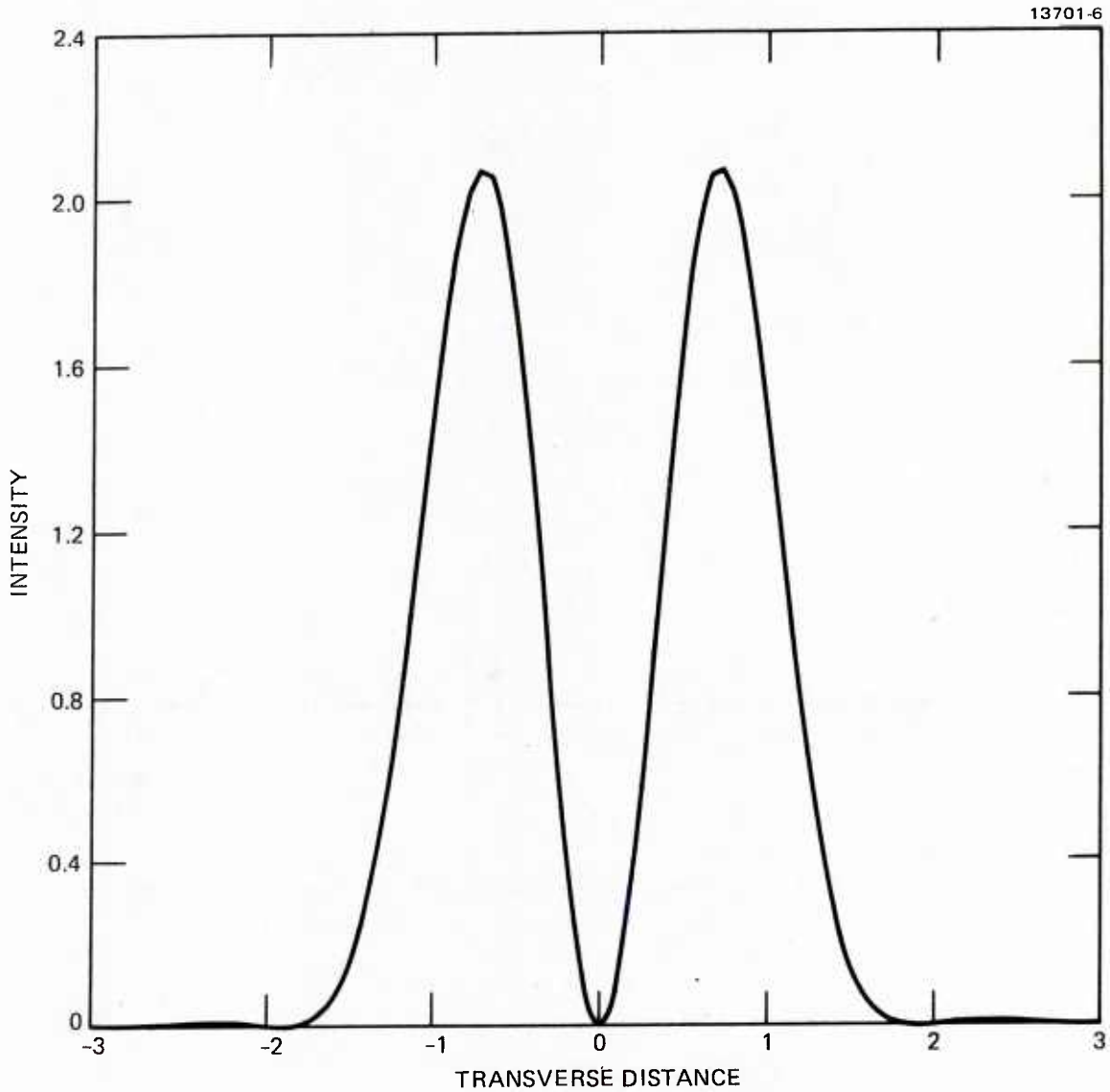

Figure 9. Output intensity for the out-of-phase case where the separation between emitters is 5 μm. Transverse distance is measured in units of $(\lambda f/2\pi a_o)$.

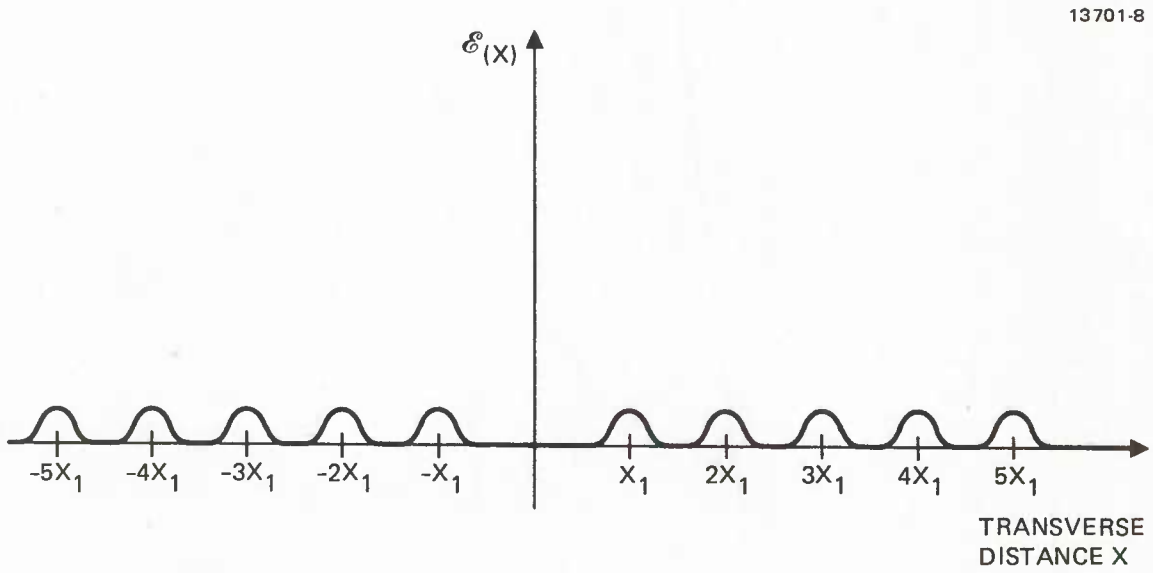

Figure 10. Input field distribution for 10 emitters which are in-phase with each other.

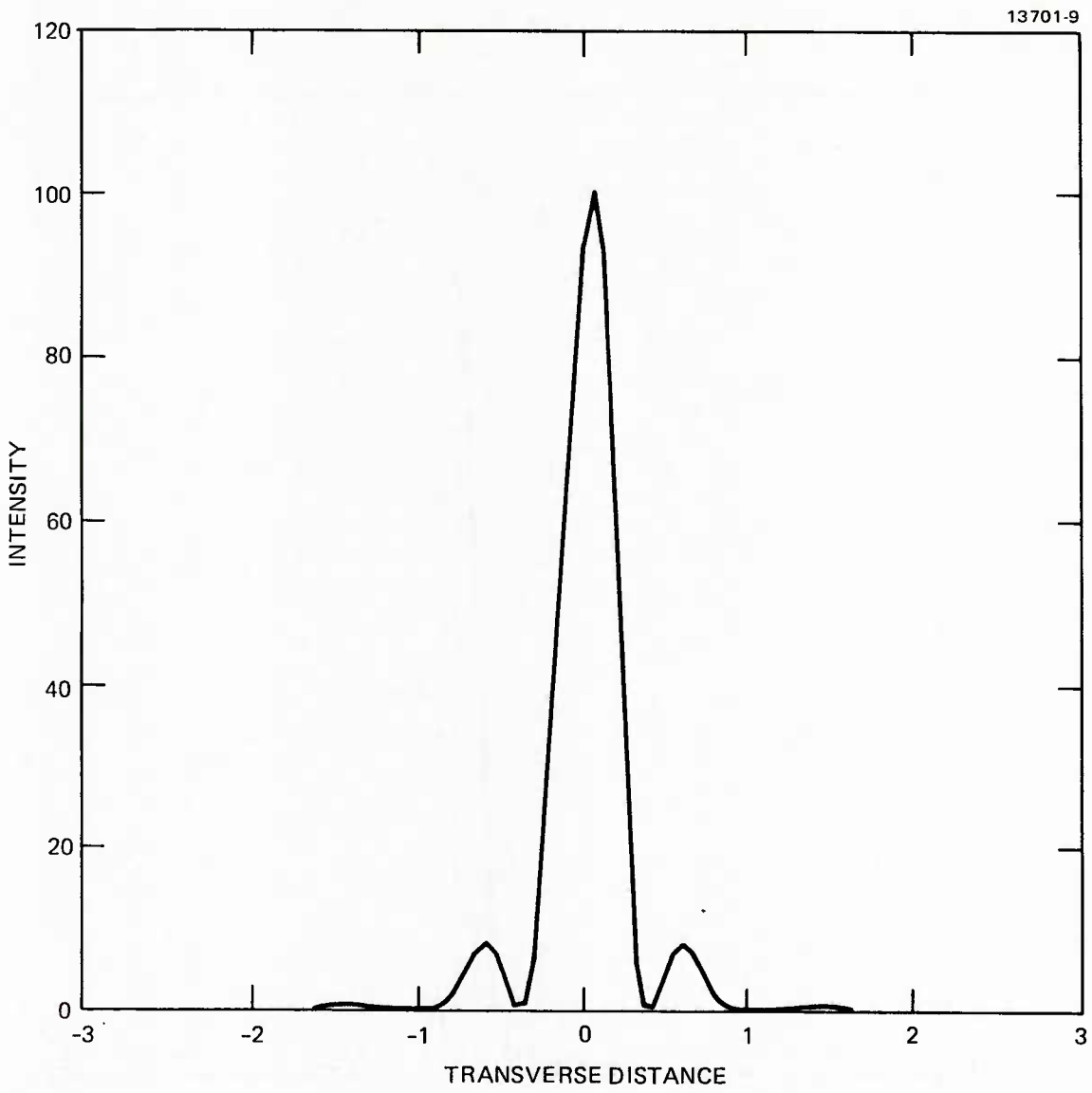

Figure 11. Output intensity for the case when the separation between in-phase emitters is 4 μm. Transverse distance is measured in units of $(\lambda f/2\pi a_o)$.

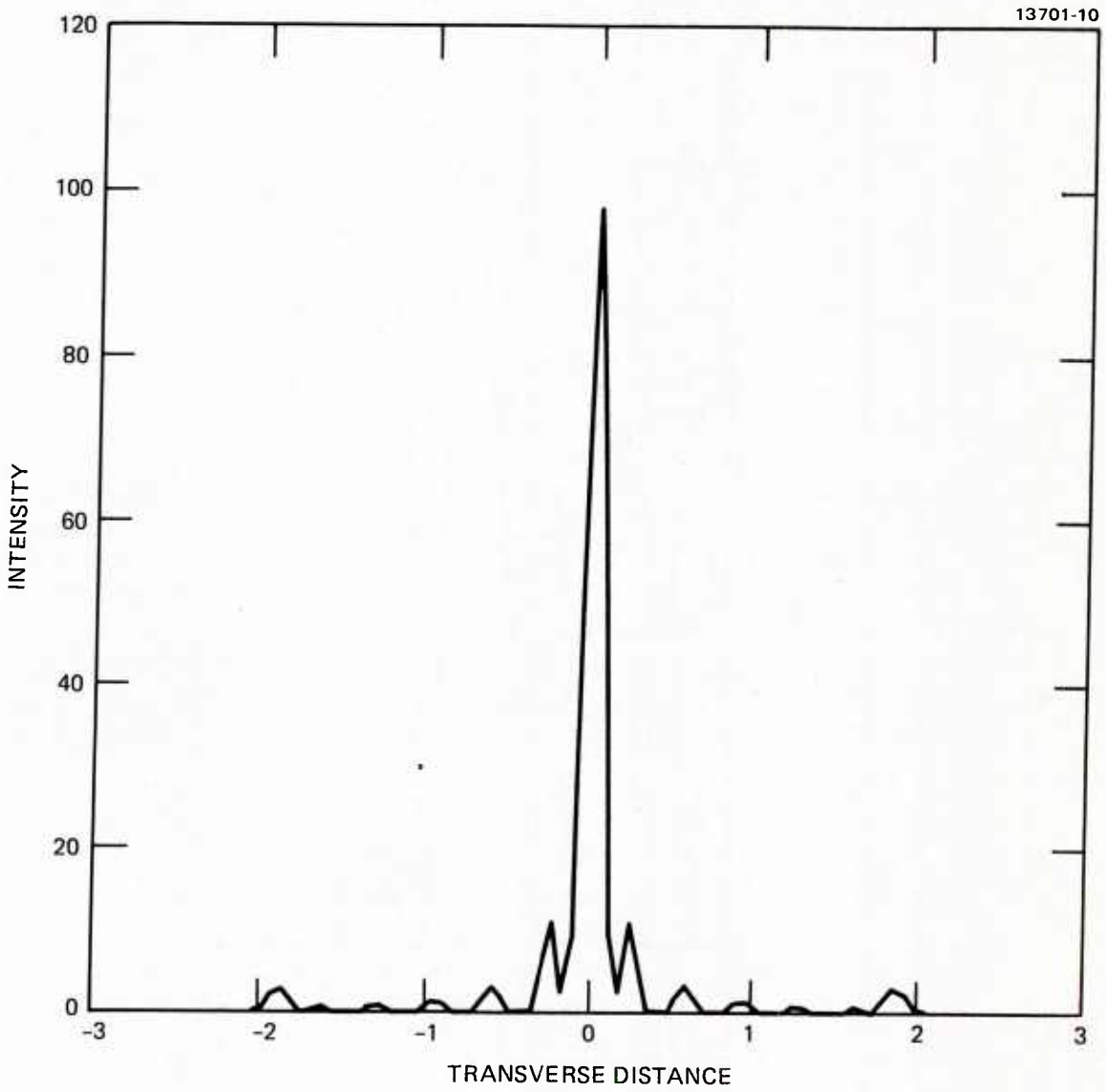

Figure 12. Output intensity for the case when the separation between in-phase emitters is 10 μm. Transverse distance is measured in units of $(\lambda f/2\pi a_o)$.

of the interference of the eletromagnetic waves. As the separation between emitters is extended from 4 μm (Figure 11) to 10 μm (Figure 12), the additional side lobes appear due to (higher order) diffraction. For the purpose of comparison, we have plotted in Figure 13 the output intensity profile for the case when the separation between the emitters is 10 μm, but the phases between them are completely random. The case where the 10-emitter system has 180° phase shift between adjacent lasers is shown in Figure 14. The output intensities are shown in Figure 15 for the case when the separation between emitters is 4 μm. Increasing the separation to 10 μm gives rise to the enhancement of certain side lobes as shown in Figure 16. The introduction of random phases yields a completely random intensity distribution as shown in Figure 17. It is interesting to note that the ten-element Xerox experiment[14] was indeed producing a diffraction-coupled phased-array laser. The output intensity of the experiment is given in Figure 18, which shows good qualitative agreement with the simple analytical modeling represented by Figure 16.

2.2 LOCKING OF MODULAR LASERS VIA PHASE CONJUGATION

As was implied in Figure 1, multiple independent gain modules can be locked in phase and frequency without mutual coupling by employing a common four-wave mixer at one end of the resonator. Alternatively, one may substitute a set of three four-wave mixers with a common pump system for the single mixer. Each separate resonator in this system forms a stable, phase-conjugate resonator in which intra-resonator aberrations are internally compensated if the output mirrors are aberration free. Further, if the output mirrors are precisely aligned with each other, i.e., if $\delta L_1 = \delta L_2 = \delta L_3$ in Figure 19, then the output fields are also in phase. Although the illustrated output mirrors are flat segments, one could substitute curved mirrors, as appropriate to a confocal resonator, for example, with the same basic locking performance.

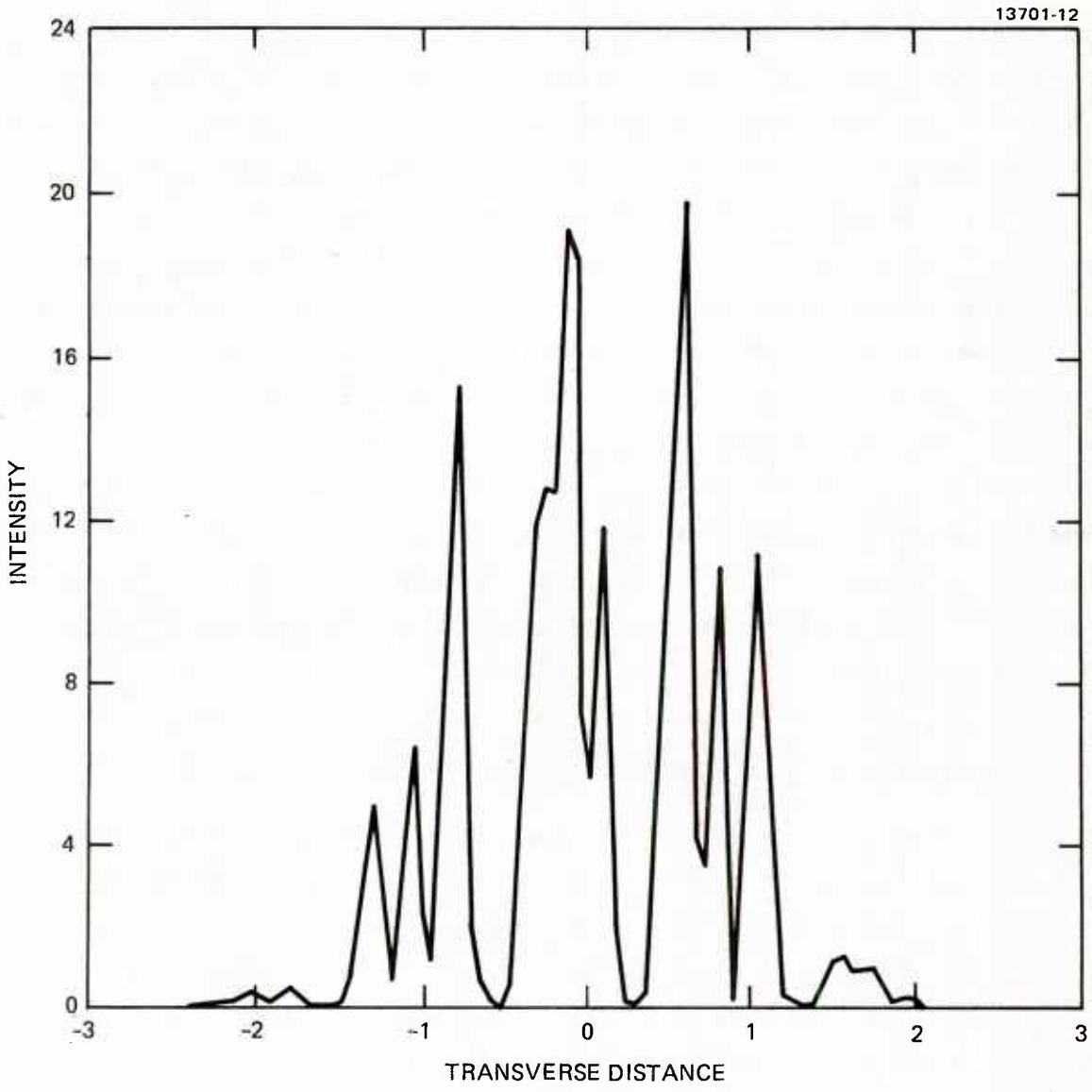

Figure 13. Output intensity of the 10-emitter system when the phases between emitters are completely random. The separation between emitters is 10 μm. Transverse distance is measured in units of $(\lambda f/2\pi a_o)$.

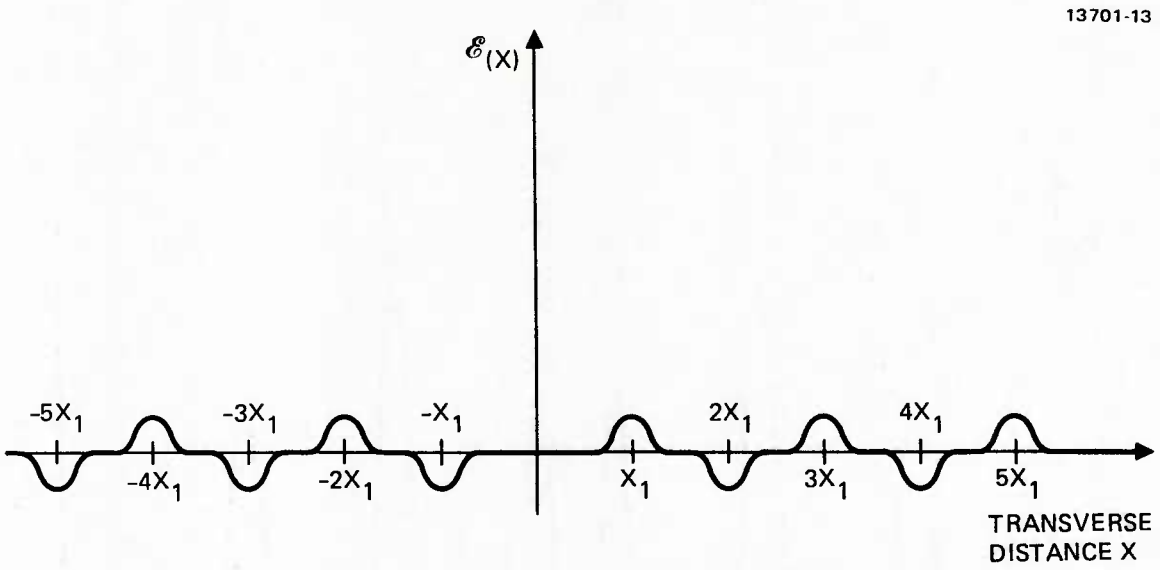

Figure 14. Field distribution for the case of 180° phase shift.

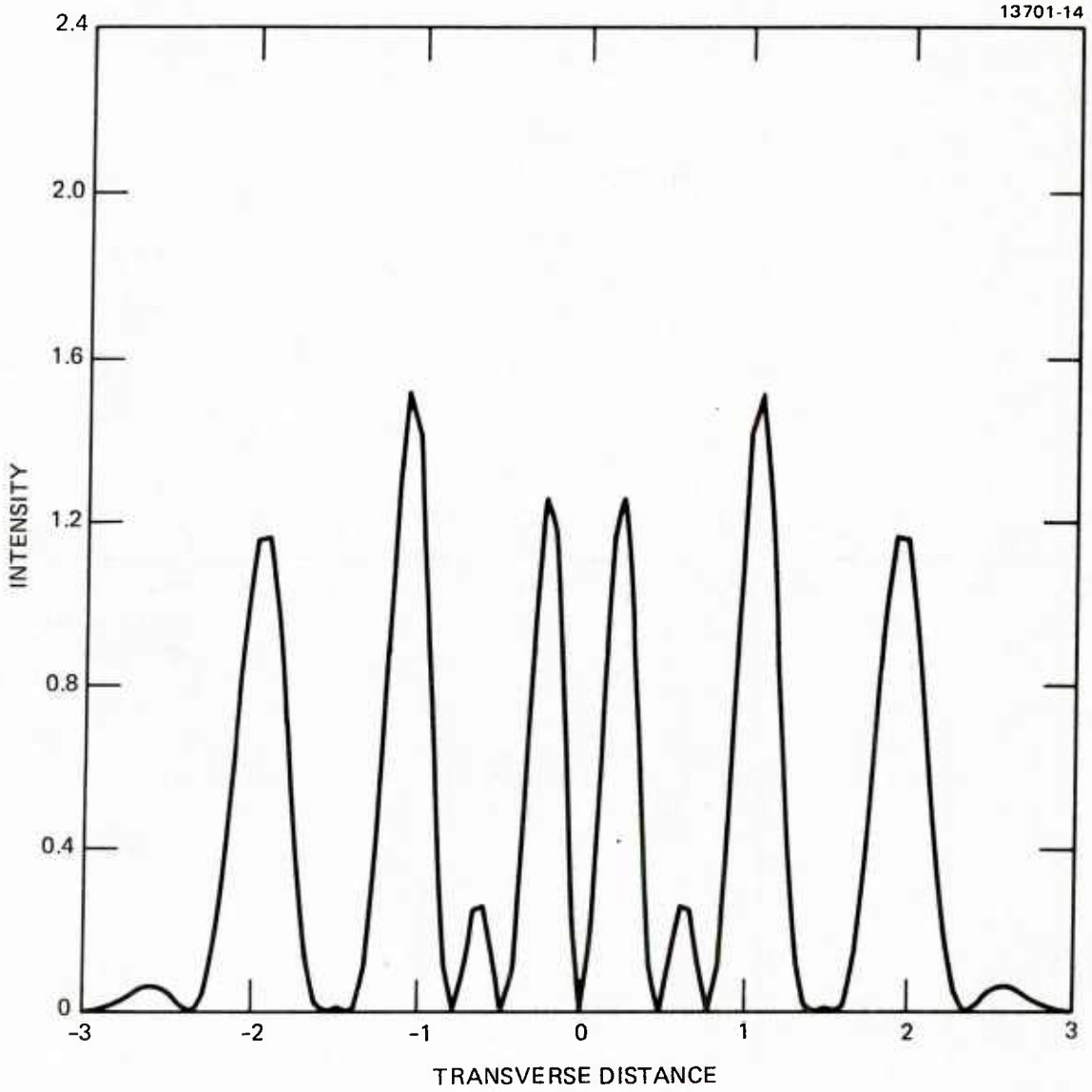

Figure 15. Intensity distribution for the case when the adjacent emitters are 180° out-of-phase and the separation between emitters is 4 μm. Transverse distance is measured in units of $(\lambda f/2\pi a_o)$.

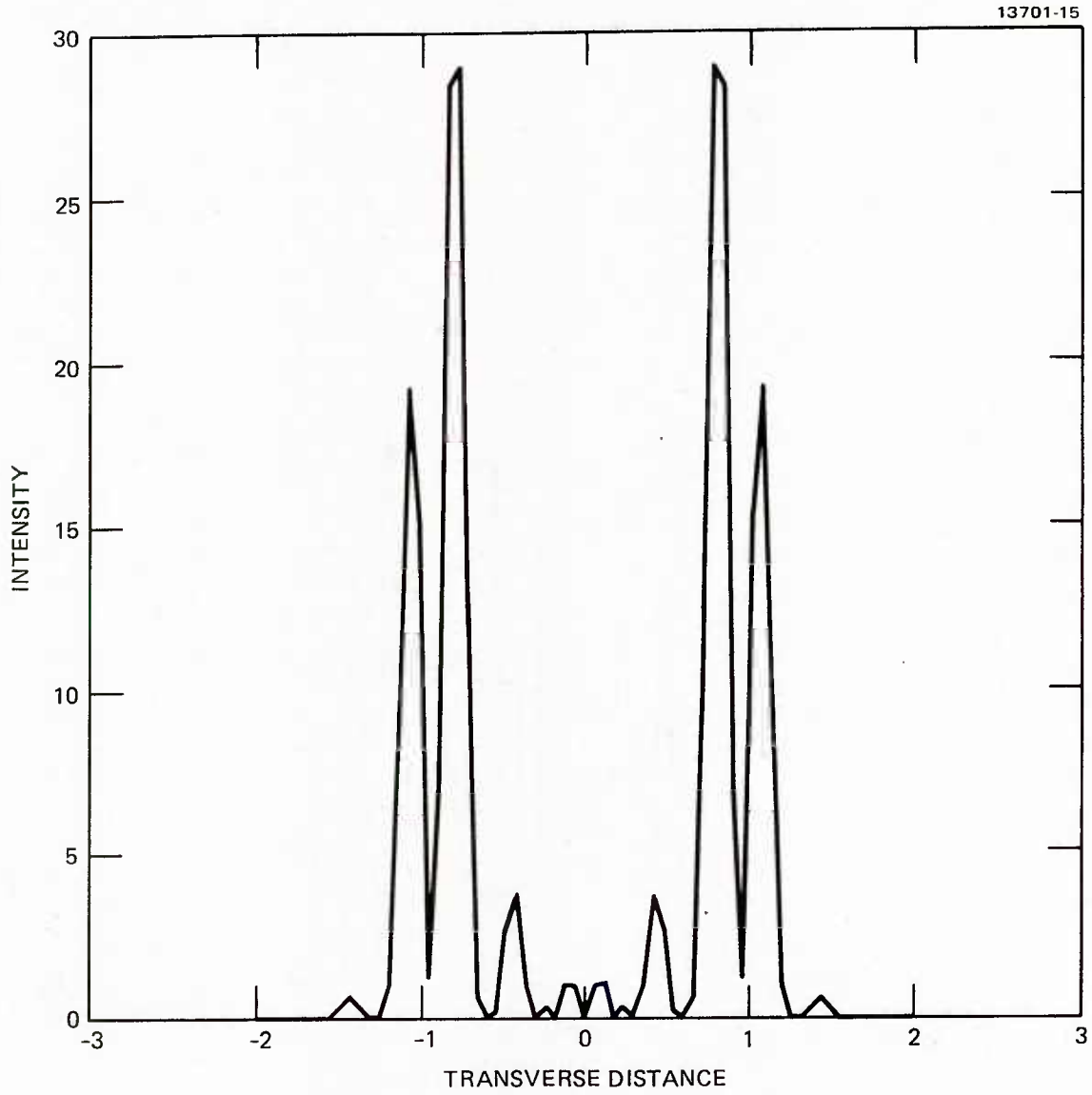

Figure 16. Intensity distribution for the case when the adjacent emitters are 180° out-of-phase and the separation between emitters is 10 μm. Transverse distance is measured in units of $(\lambda f/2\pi a_o)$.

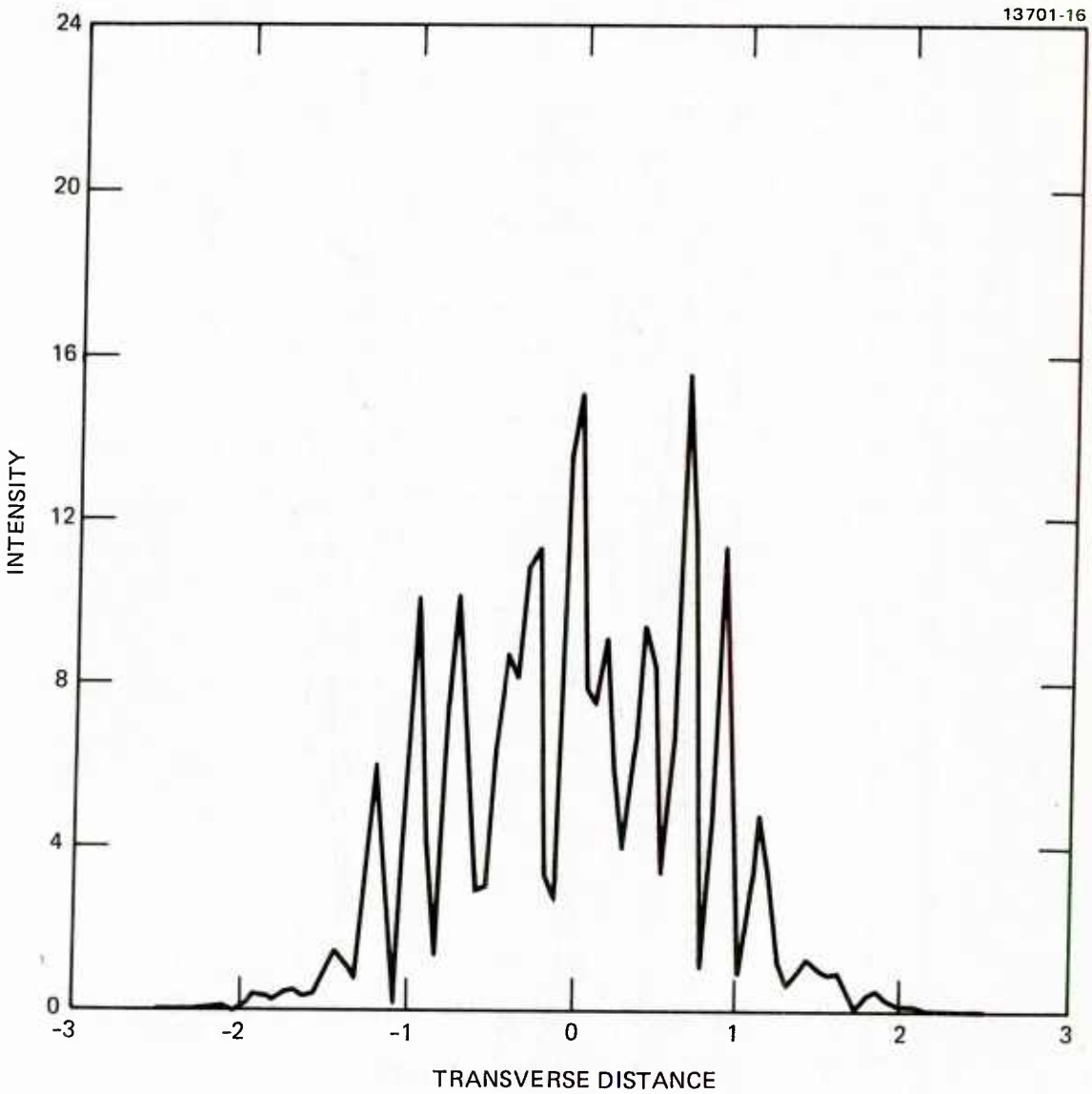

Figure 17. Intensity distribution for the case when the 10-emitter system has random phases among all emitters. Transverse distance is measured in units of $(\lambda f/2\pi a_o)$.

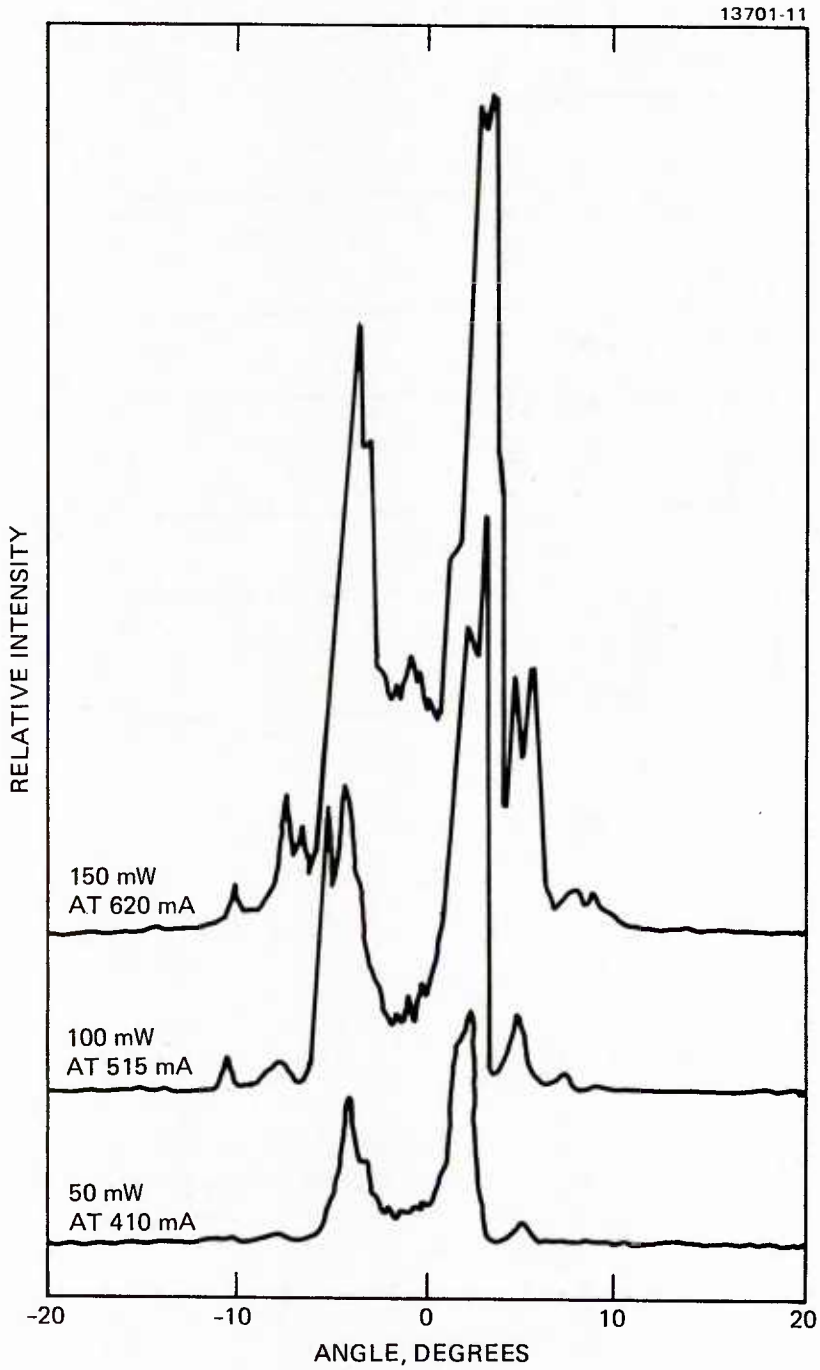

Figure 18. The output intensity of the Xerox phased array diode laser. (From Reference 14). Curves corresponding to different output powers have been separated vertically for clarity.

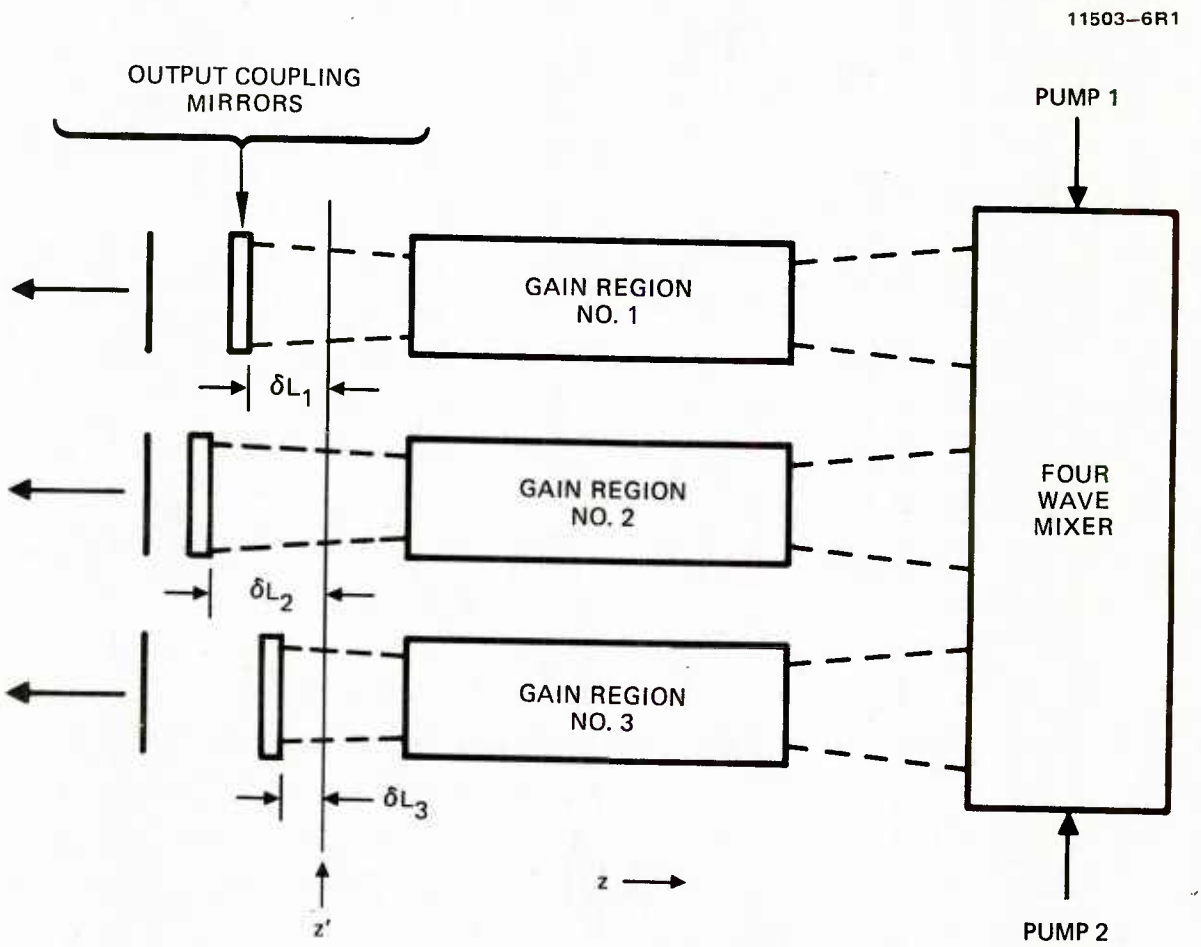

Figure 19. Geometry of the phase locking analysis with a four-wave-mixer conjugation locking technique.

In order to analyze the requirements needed to achieve a high quality output beam, consider the field at an arbitrary plane, located at position z', inside of each resonator, as illustrated in Figure 19. The three output coupling mirrors are assumed to be spaced from this plane by variable distance δL_n. Ignoring transverse wavefront variations, the field incident on plane z' from the right has a complex amplitude A_n' where

$$A_n' = Ae^{-i\phi_n(z')} \quad , \tag{7}$$

where A is a scaler and ϕ_n is a phase shift which is to be determined. After reflecting off the output coupling mirror and returning to plane z', the field amplitude is:

$$A_n'' = A\sqrt{R_m}\exp\left[-i(\phi_n(z') - 2k\delta L_n + \phi_m)\right] \quad , \tag{8}$$

where ϕ_m is the mirror-induced phase shift and R_m is the power reflectivity of the output mirror.

After amplification and reflection from the conjugator, followed by reamplification, the returning field at plane z' has a complex amplitude A_n''', where

$$A_n''' = A\sqrt{R_m R_c G_s}\ \exp\left[i(\phi_n(z') - 2k\delta L_n + \phi_m + \phi_{n1} + \phi_{n2})\right] \quad , \tag{9}$$

where G_s is the steady state round-trip power gain of the amplifier, R_c is the conjugator reflectivity, and ϕ_{n1} and ϕ_{n2} are the phases of pumps 1 and 2, respectively. After many iterations, the oscillation condition requires that $A_n''' = A_n'$, so that

$$\sqrt{R_c\ R_m\ G_s} = 1 \quad , \tag{10}$$

and

$$\phi_n(z') = 1/2\ [-2k\delta L_n + \phi_m + \phi_{n1} + \phi_{n2}] \quad . \qquad (11)$$

Thus, if the output mirrors are aligned so that all δL_n are equal, and if ϕ_m is the same for all mirrors, and if the mixer pumping is coordinated so that $\phi_{n1} + \phi_{n2}$ is the same for all four-wave mixers, then all three phases $\phi_n(z')$ are equal. That is, the output wavefront is coplanar. The fact that the output phase front is not flat if the end mirrors are offset from each other is analogous to the situation on a standard PCR with an aberrated out-coupling mirror. In this case, it has been shown that the phase of the out-coupled wave matches the distortion of the mirror.[15] The impact of this analysis on coherent phasing of multiple GaAs diodes is either that one well-figured mirror must be used for the whole array or that the separate end mirrors must be precisely aligned to much better than a wavelength.

Preliminary three-dimensional computer calculations of a multiple diode PCR show that the output of such a resonator is virtually independent of refractive index and length variations of the individual diodes. Figure 20 shows the amplitude and phase of a converged solution to the resonator shown in Figure 19 at various locations in the resonator. Parameters used for this sample calculation are:

Wavelength	840 nm
Diode cross section	13.50 x 40 μm
Gain-length product	0.50
Saturation intensity	40.00 kW/cm^2
Distance to conjugator	500.00 μm
Output coupling	50 percent

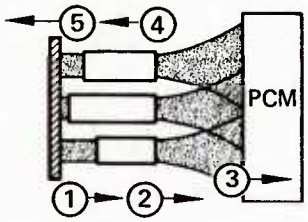

(a) 3-DIODE PHASE CONJUGATE RESONATOR

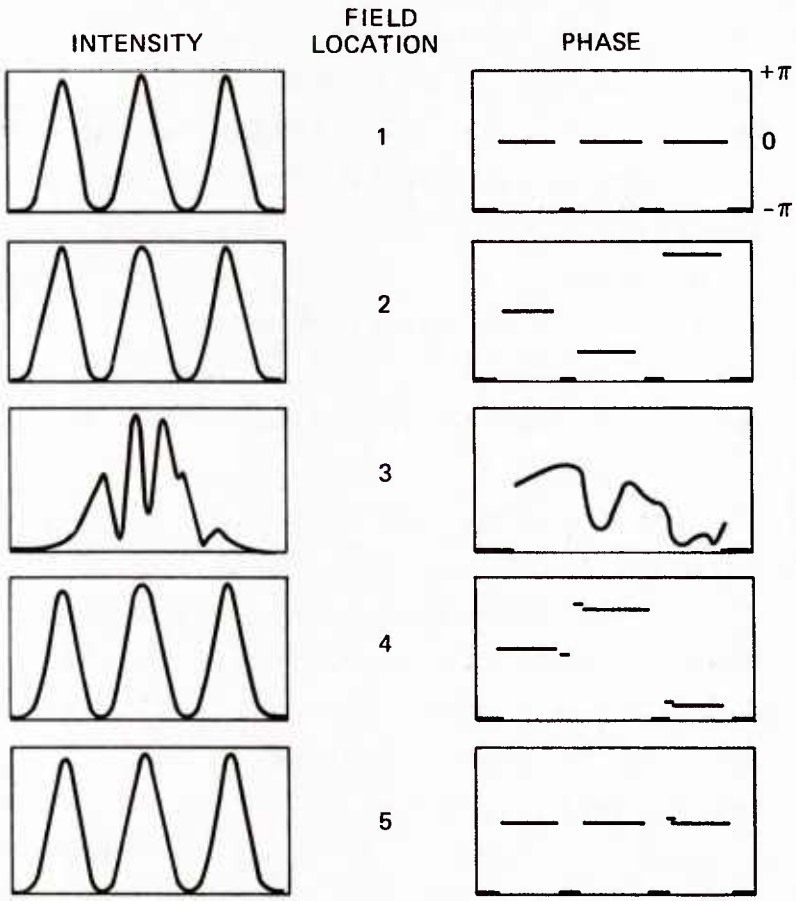

(b) INTRA-CAVITY INTENSITY AND PHASE

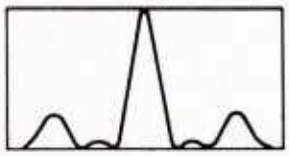

(c) OUTPUT FAR-FIELD INTENSITY

Figure 20. Computer calculations showing intensity and phase at different locations for a three-diode phase conjugate resonator. Phase distortions arise from different diode lengths.

Despite diode-to-diode phase variations of more than half a wave, the output is flat. For a single diode of the same characteristics, the output amplitude and phase are given in Figure 21. The total power extracted from one diode is 17 mW while from three diodes 47 mW is extracted. The loss in extraction efficiency per diode in the array is less than 8 percent. For multimode waveguide diodes the loss should be even smaller.

Calculations have also been performed with a conventional mirror in place of the PCM. Even with no phase variations between the diodes, the output is poor as shown in Figure 22 which gives the far-field irradiance pattern of this calculation after twenty iterations. The pattern is clearly inferior, and furthermore the power is less than 1 mW at this iteration.

2.3 BEAM COMPACTING SYSTEMS FOR HIGH QUALITY FAR-FIELD PERFORMANCE

Arrays of laser diodes must necessarily be packed with appreciable spacing between the diodes (relative to the diode size) in at least one dimension - the narrow dimension of the diode. In order to cool the diodes better, it may also be important to space the diodes in the direction of the long dimension of the diode. Since far-field power combining appears to be the most expedient and efficient technique for combining the power outputs of N diodes, it is important to examine the impact of a widely spaced set of radiation sources on the far-field distribution. This is an extremely important consideration in diode arrays intended to drive nonlinear optical devices, since such systems typically focus the available power into the nonlinear crystal in order to generate sufficient optical intensity to achieve efficient doubling. The field distribution at the focus is essentially a far-field pattern.

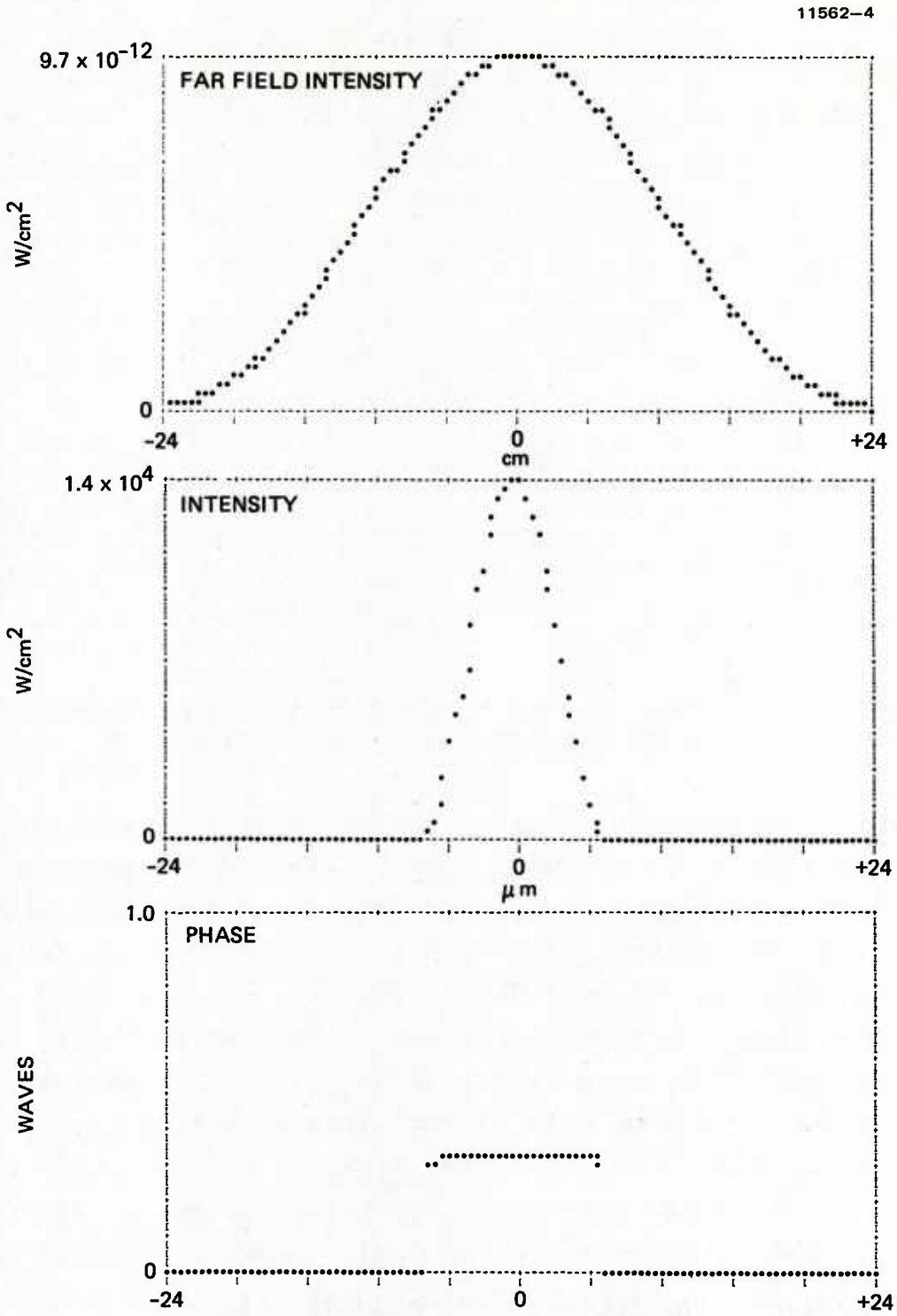

Figure 21. Output intensity and phase of a single diode. (Computer simulation)

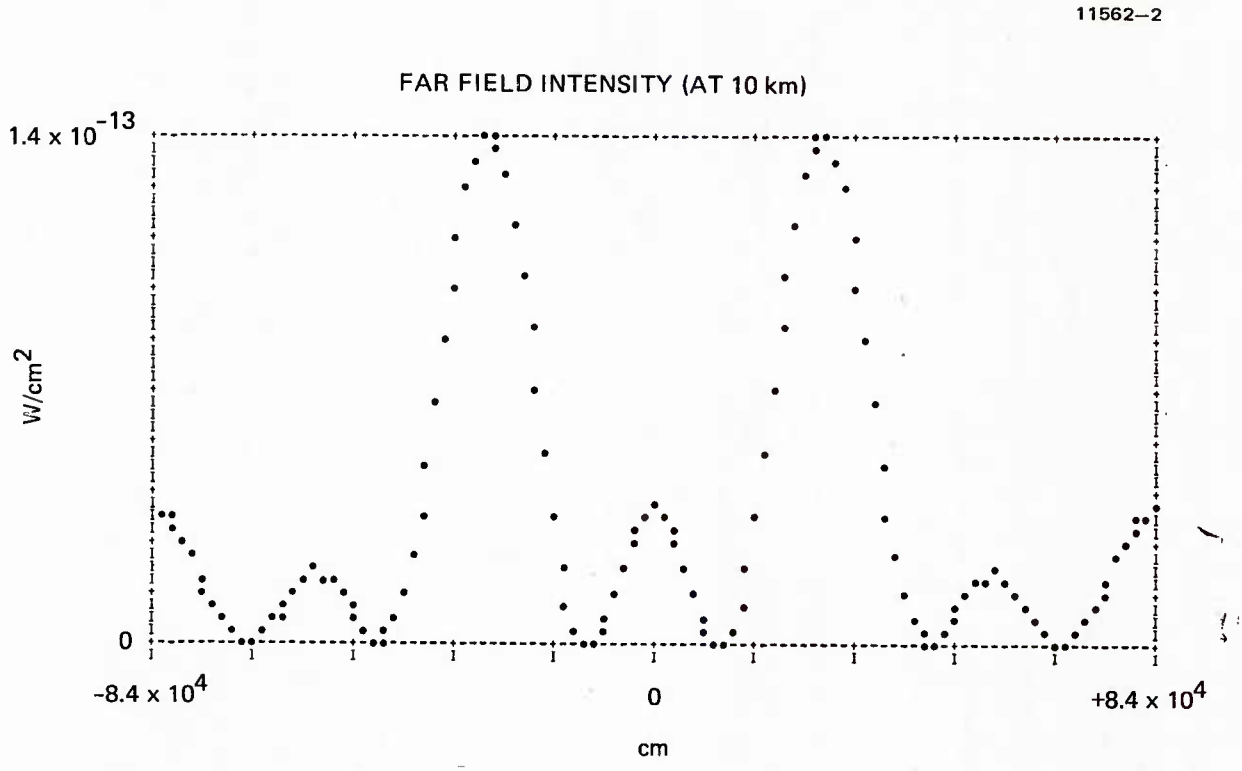

Figure 22. Far-field intensity of a 3-diode laser with a conventional feedback mirror.

Assuming that the diode array is arranged on a periodic lattice, as viewed end-on, with appreciable spacing between elements, then the radiating source resembles a diffraction grating. It is well known that the far-field pattern of such a uniphase source also has a quasi-periodic character with a period determined by the inverse of the spacing between diodes, as exhibited in Figure 23b, which is taken from Reference 16. This pattern consists of a major lobe on axis plus a large number of similarly shaped secondary or "grating" lobes with the nearby lobes of comparable size to the main lobe (for large percentage diode spacings). Unfortunately, for the diode spacings required in our modular laser application, most of the far-field power is contained in the composite of the grating lobes rather than in the main lobe. In the practical applications, the power in these grating lobes will effectively be lost.

11562-14

A. NEAR FIELD INTENSITY
WELL ALIGNED ARRAY

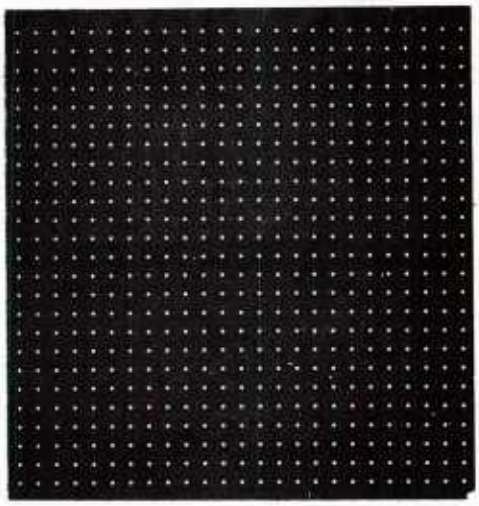

B. FAR FIELD INTENSITY
WELL ALIGNED ARRAY

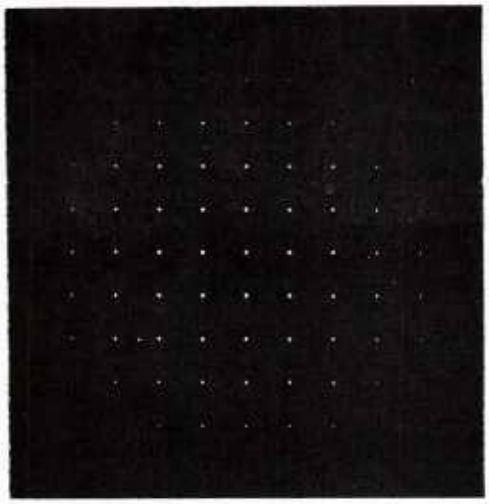

C. NEAR FIELD INTENSITY
POORLY ALIGNED ARRAY

D. FAR FIELD INTENSITY
POORLY ALIGNED ARRAY

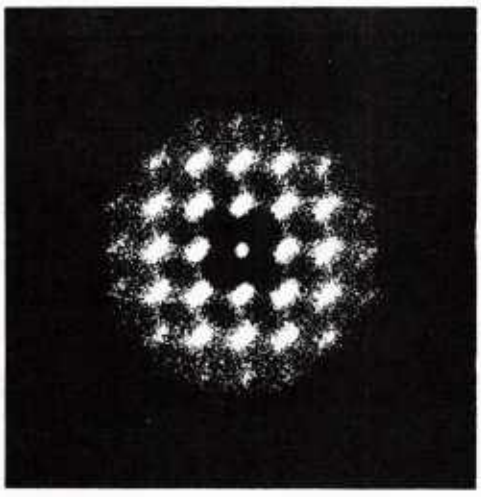

Figure 23. Near- and far-field patterns of well aligned and poorly aligned arrays (after Ref. 16).

Randomizing the position of the diodes destroys the periodicity of the source, and of the far-field pattern as well, such that the side lobe peaks are less intense than with the periodic array. This is dramatically illustrated in Figure 23d. Unfortunately, the total power which is lost from the main lobe, given the same average diode spacing, is unchanged by the randomization. This loss is determined almost entirely by the area thinning factor of the diode array, which is defined as the ratio of the total diode effective radiating area to the area of the box encompassing the diode (end face) array. The effective intensity is directly proportional to the thinning factor. Thus for a thinning factor of 50%, half of the radiated power is contained in the side lobe structure and is thereby lost to the main lobe, insofar as the diodes maintain their average spacing under randomization.

The only workable solution to this problem for a given diode spacing is to use mirrors (Figure 24a) or lenses (Figure 24b), or some combination of these techniques, to redistribute the diode near-field pattern in such a way that a more compact radiating source is produced. The mirror systems illustrated in Figure 24a tend to produce unequal path differences which could, in principle, be compensated with optical glass slabs of differing length. However, precision brute force path matching seems extremely difficult. Similar path matching problems occur for the lens arrays shown in Figure 24b. One major advantage of using a phase conjugate resonator (PCR) in this diode coupling application is that these path length differences are automatically cancelled out if the beam combining optics are placed within the PCR.

2.4 NORMAL MODES OF A MULTIPLE-ELEMENT PLANAR WAVEGUIDE

This section presents calculations of the normal modes of a set of coupled emitters. This analysis is relevant to coupling schemes such as the use of a phase conjugate resonator or evanescent-wave coupling. In such schemes, the output of a phased-array laser system can be considered in terms of the superposition of the normal modes of their respective

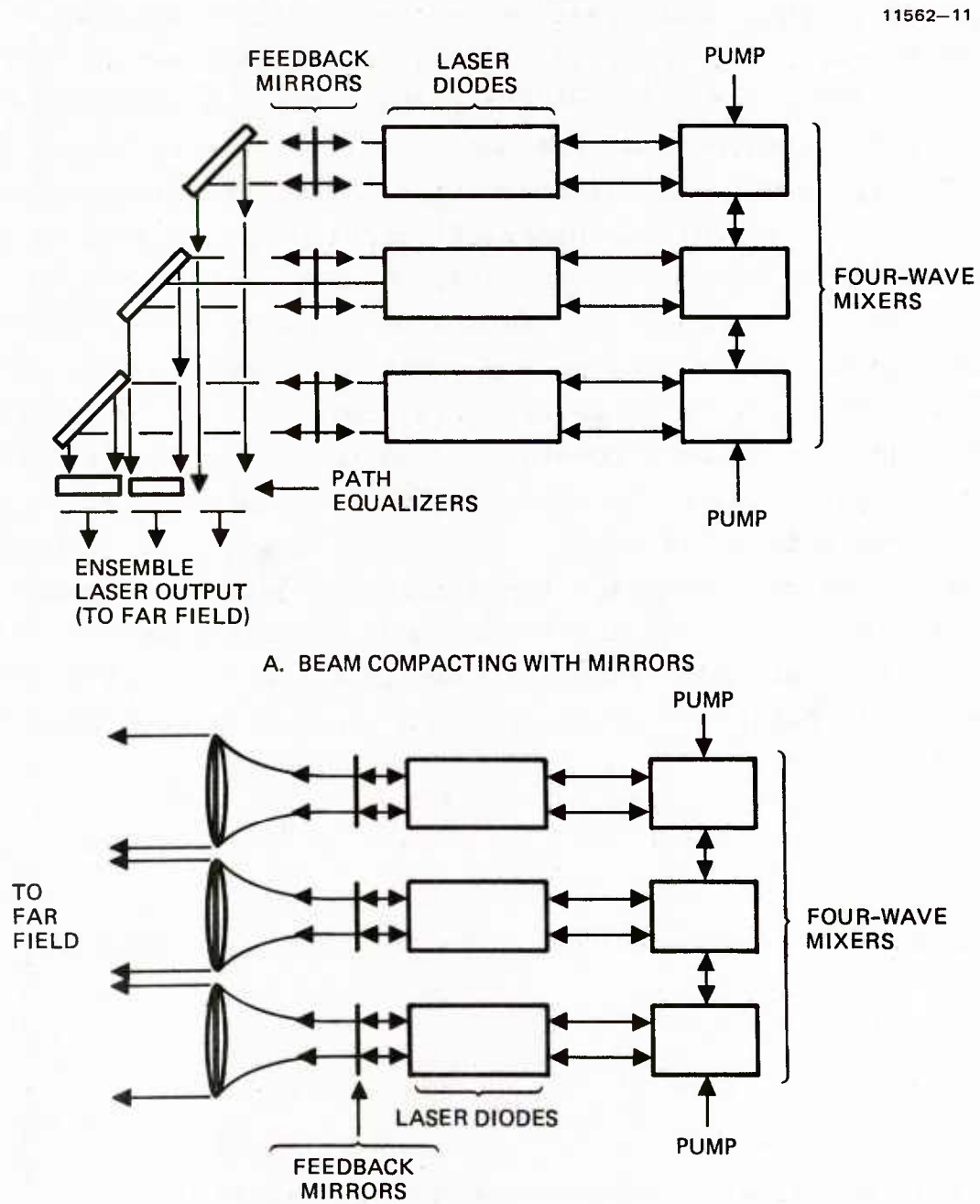

Figure 24. Beam compacting systems for diode-laser arrays. The feedback mirrors may be moved to the left of the beam-compacting elements in order to compensate for optical path differences.

waveguide system. This picture has certain limitations. It cannot be rigorously applied to a saturated gain medium due to the nonlinear nature of the index of refraction; i.e., the detuning of the stimulated photon from the transition resonance gives rise to an effective nonlinear susceptibility. The saturated regime poses an extremely difficult mathematical problem. Only recently, numerical solutions have been obtained that provide a good physical insight into the role of the saturated index of refraction on the transverse mode of a single gain medium.[17] However no work has been done on an array of laser oscillators. Hence, we would like to provide a first step toward the understanding of the behavior of phased-array lasers by analyzing the multiple waveguide problem. This approach is valid for the linear and homogenous gain regime. By homogenous gain we shall imply that the gain coefficient is constant for each laser and is the same for all lasers.

The problem under consideration is illustrated in Figure 25. The starting point of the analysis is the scalar wave equation

$$\left\{\nabla^2 + \frac{\omega^2}{c^2} \quad n^2\right\} \quad E \quad = \quad 0 \tag{12}$$

in the harmonic approximation. The scalar field can be written as

$$E \quad = \quad \frac{1}{2} \quad \{\mathscr{E}(x,z) \quad e^{i\beta z} + c.c.\} \tag{13}$$

such that the slowly varying envelope approximation

$$\left|\frac{d\mathscr{E}}{dz}\right| \quad << \quad \beta \quad |\mathscr{E}| \tag{14}$$

is satisfied. Equation (14) implies that both the amplitude and phase of the complex envelope $\mathscr{E}$ vary slowly compared to the

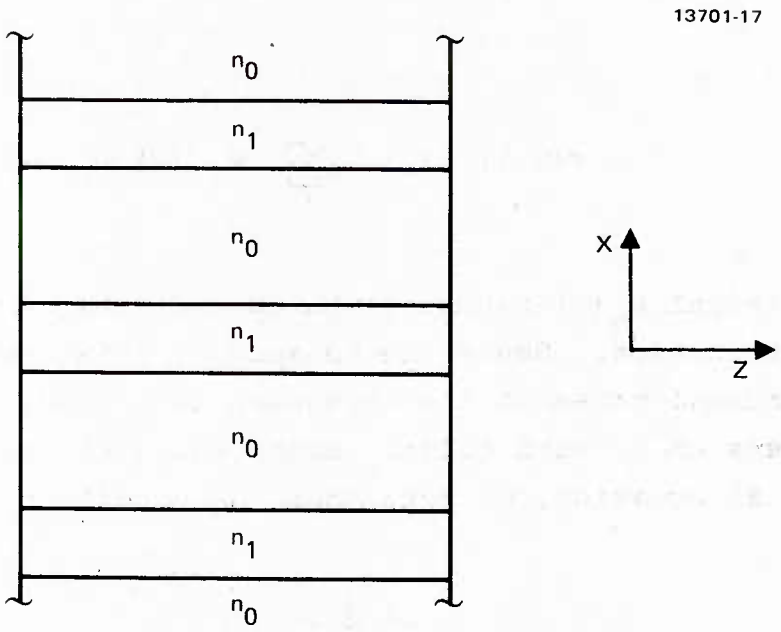

Figure 25. Geometry for the multiple planar waveguide. n_0 and n_1 are the indices of refraction.

effective wavelength β^{-1} of the waveguide. Application of Eqs. (13) and (14) to the wave Eq. (12) yields

$$2i\beta \frac{\partial \mathcal{E}}{\partial z} + \frac{\partial^2}{\partial x^2} \mathcal{E} + \left(\frac{\omega^2}{c^2} n^2 - \beta^2 \right) \mathcal{E} = 0 \qquad (15)$$

which is just the quasi-optical or paraxial wave equation. Eq. (15) has been the starting point of numerous numerical simulations of propagation in optical fiber systems.[18] The normal modes u of the system are defined to be the solutions of

$$\frac{\partial^2}{\partial x^2} u + \left(\frac{\omega^2}{c^2} n^2 - \beta^2 \right) u = 0 \qquad (16)$$

Any general wave can be written as a superposition of the normal modes

$$\mathcal{E}(x,y) = \sum_{\alpha} A_{\alpha}(z)\, u_{\alpha}(x) \tag{17}$$

The coeffieicnt $A_{\alpha}(z)$ can be computed in terms of the initial field distribution. Hence the essence of this section is to calculate the normal modes of the waveguide as a function of the transverse dimension of each guide. Since Eq. (16) is a second-order differential equation, we note that the condition

$$\frac{\omega^2}{c^2} n^2 - \beta^2 > 0 \tag{18}$$

is required for the existence of confined modes, and

$$\frac{\omega^2}{c^2} n^2 - \beta^2 < 0 \tag{19}$$

is required for the existence of unconfined modes. Since the indices of refraction are chosen such that for n_1 the situation corresponding to Eq. (18) is satisfied, while for n_0 condition Eq. (19) is satisfied, we are dealing with a configuration shown in Figure 26. Boundary conditions must then be satisfied; they are given by

$$\left.\begin{array}{l} u(x) \\ \\ \dfrac{du}{dx} \end{array}\right\} \quad \text{continuous at the boundary} \tag{20}$$

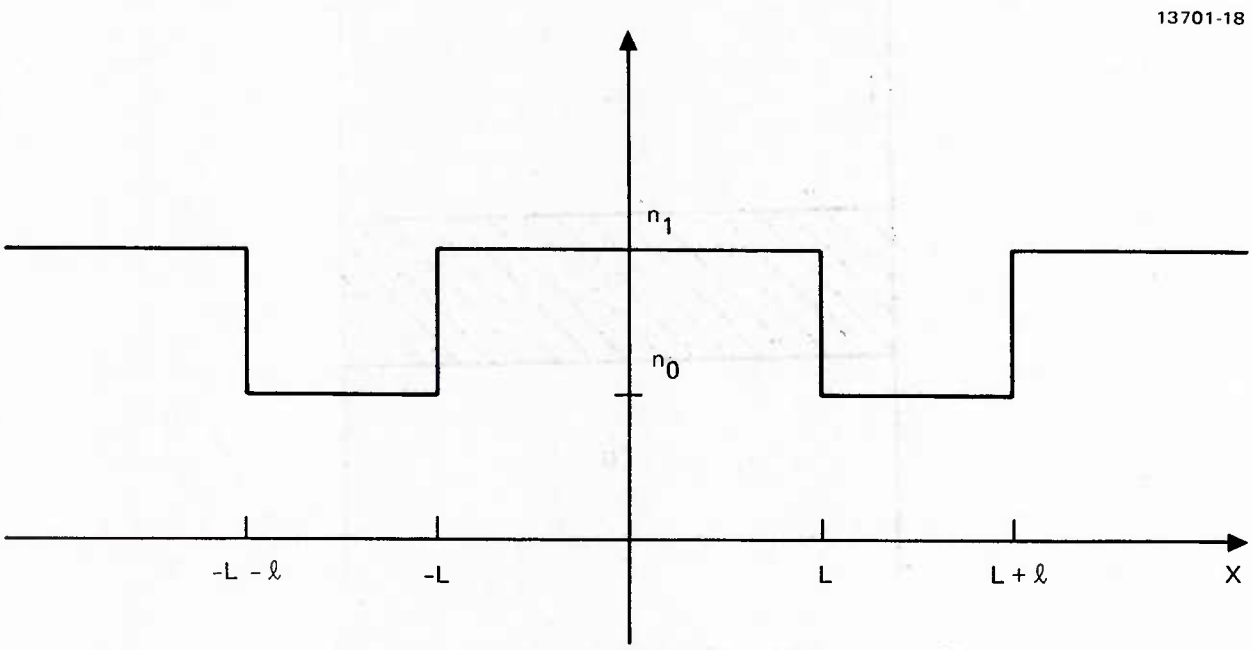

Figure 26. Relative size of the indices of refraction for the distinct waveguides.

In the same spirit as in Section 2.1, we shall build our knowledge by solving relatively simple problems first. In this context, we consider the normal modes of a single planar waveguide whose geometry is shown in Figure 27. We shall assume that the distribution of the magnitudes of the index of refraction are such that $n_1 > n_0$, as shown in Figure 28. Hence, the effective wavenumbers are defined such that

$$k_1^2 = \frac{\omega^2}{c^2} n_1^2 - \beta^2 > 0, \quad |x| < L$$

$$-k_0^2 = \frac{\omega^2}{c^2} n_0^2 - \beta^2 < 0, \quad |x| > L \tag{21}$$

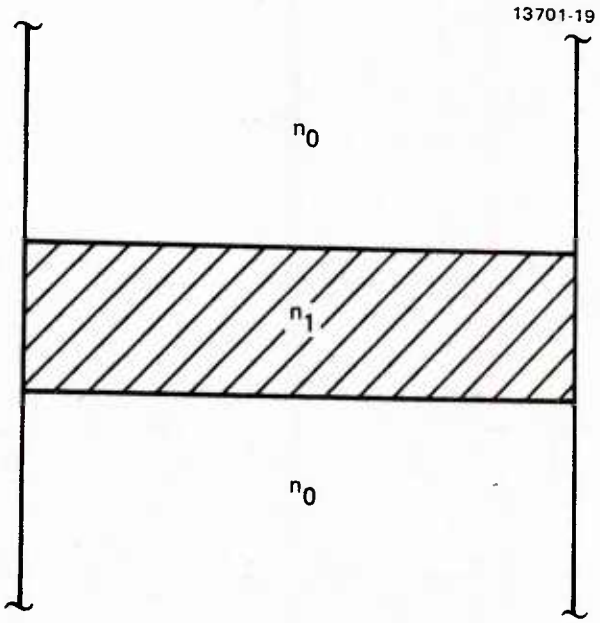

Figure 27. Geometry of the single planar waveguide.

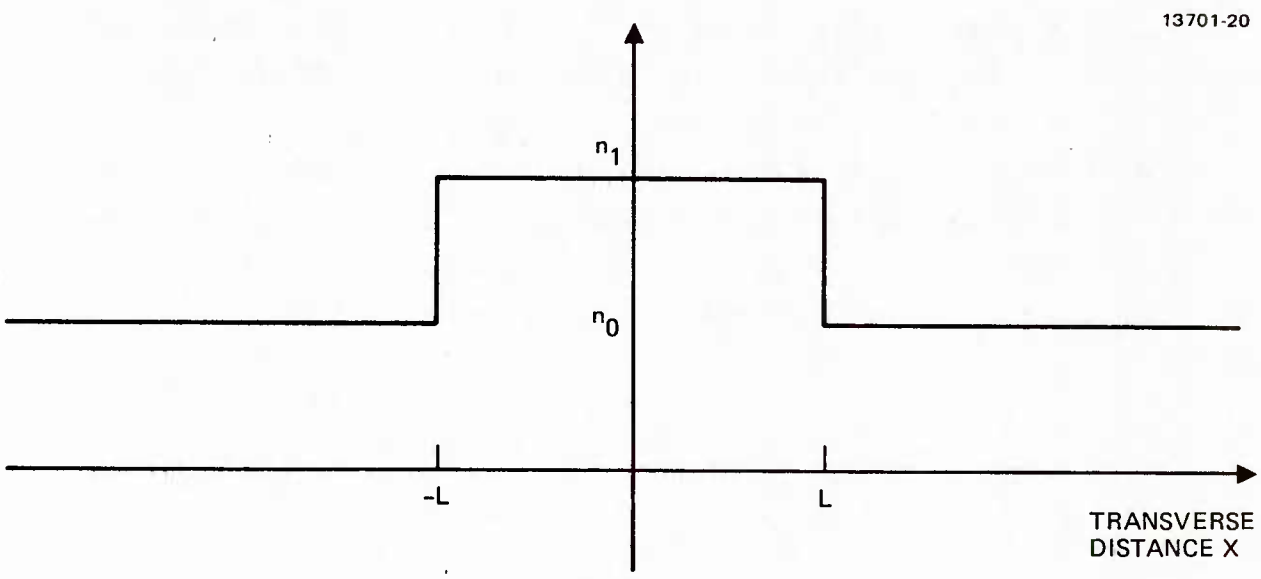

Figure 28. Relative sizes of the index of refraction for the single planar waveguide case.

The solutions can be obtained by inspection. They are

$$u(x) = A\, e^{k_0 x},\ x < -L$$

$$u(x) = \begin{cases} B \cos k_1 x \\ C \sin k_1 x \end{cases} \quad |x| < L \tag{22}$$

$$u(x) = D\, e^{-k_0 x},\ x > L$$

Applying the boundary conditions at $x = L$, one finds the following dispersion relations

$$\begin{aligned} \tan k_1 L &= \frac{k_0}{k_1}, \text{ even solution} \\ \tan k_1 L &= \frac{k_1}{k_0}, \text{ odd solution} \end{aligned} \tag{23}$$

By even solution, we mean the cosine function solutions in the region $|x| < L$, while odd solutions are represented by sine functions in the same region. The dispersion relations determine precisely the number of modes available for a specific transverse dimension L. Figures 29 and 30 show the plot of the lowest order for the even and odd modes, respectively.

Next, we consider the normal modes of the double planar waveguide whose gemoetry is shown in Figure 31. The relative indices of refraction are shown in Figure 32. Following the same procedure as outlined above the solutions are

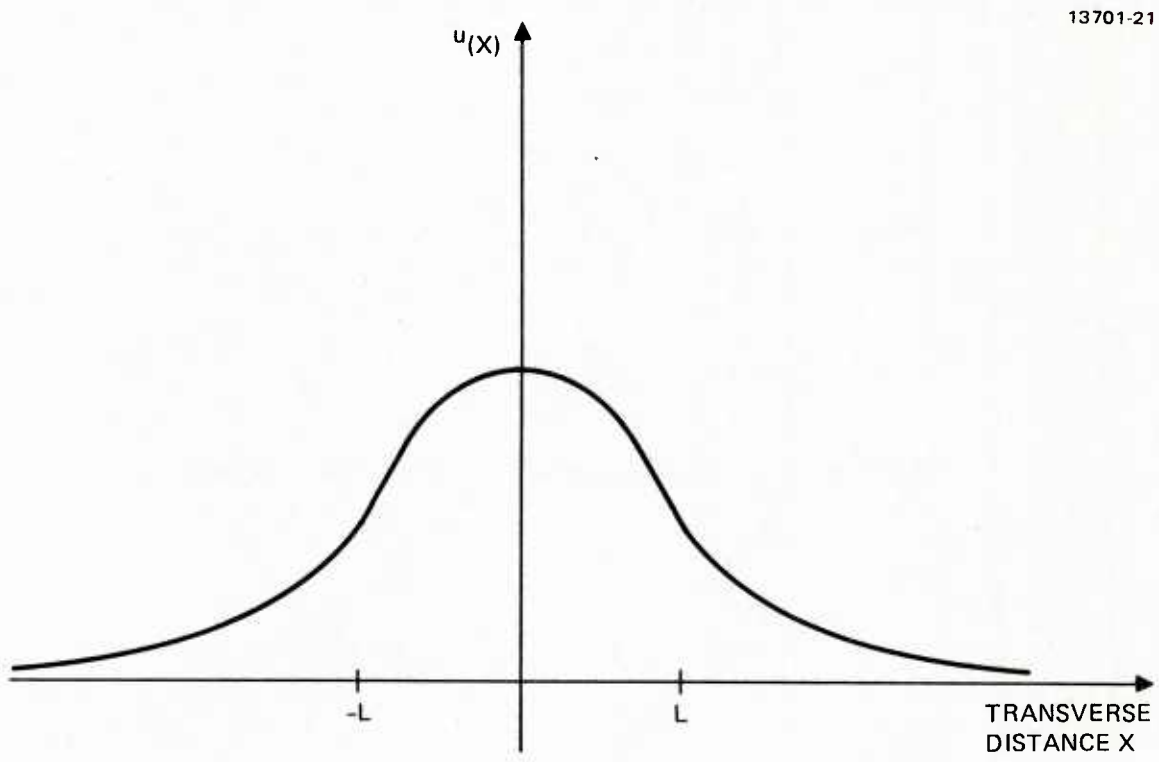

Figure 29. Lowest order even mode.

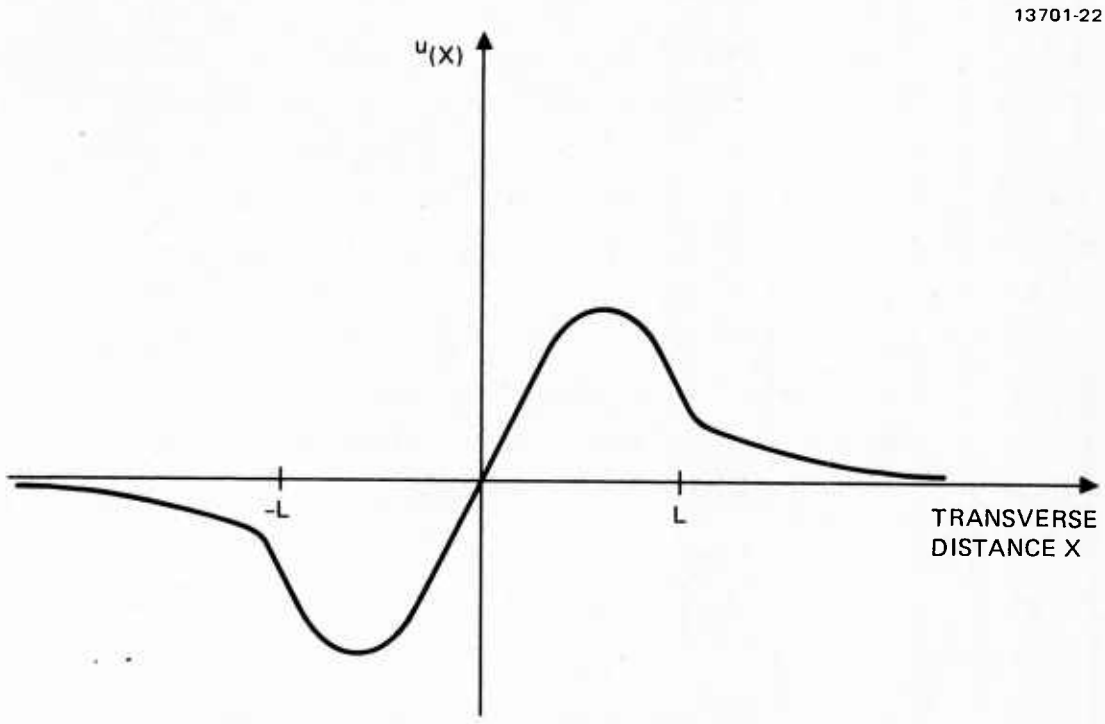

Figure 30. Lowest order odd mode.

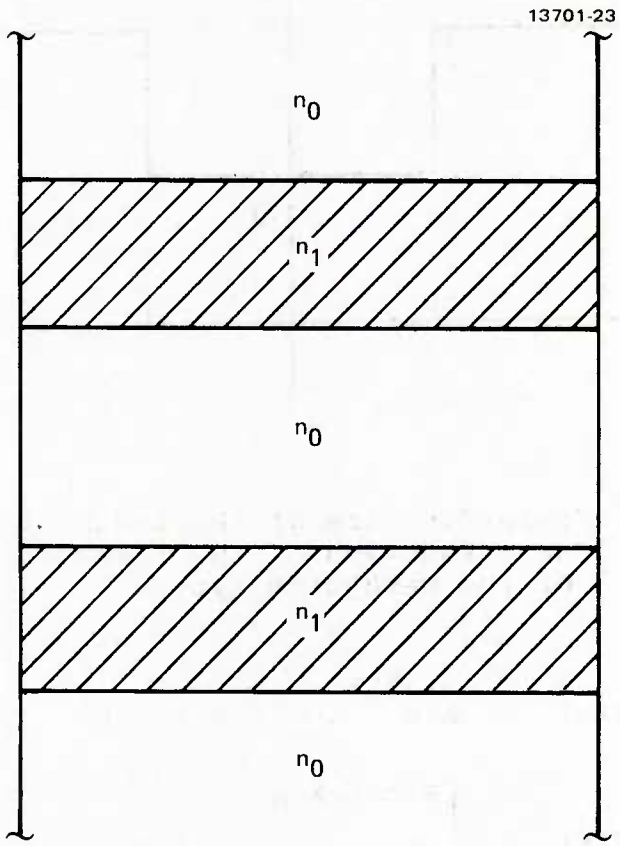

Figure 31. Geometry for the double planar waveguide.

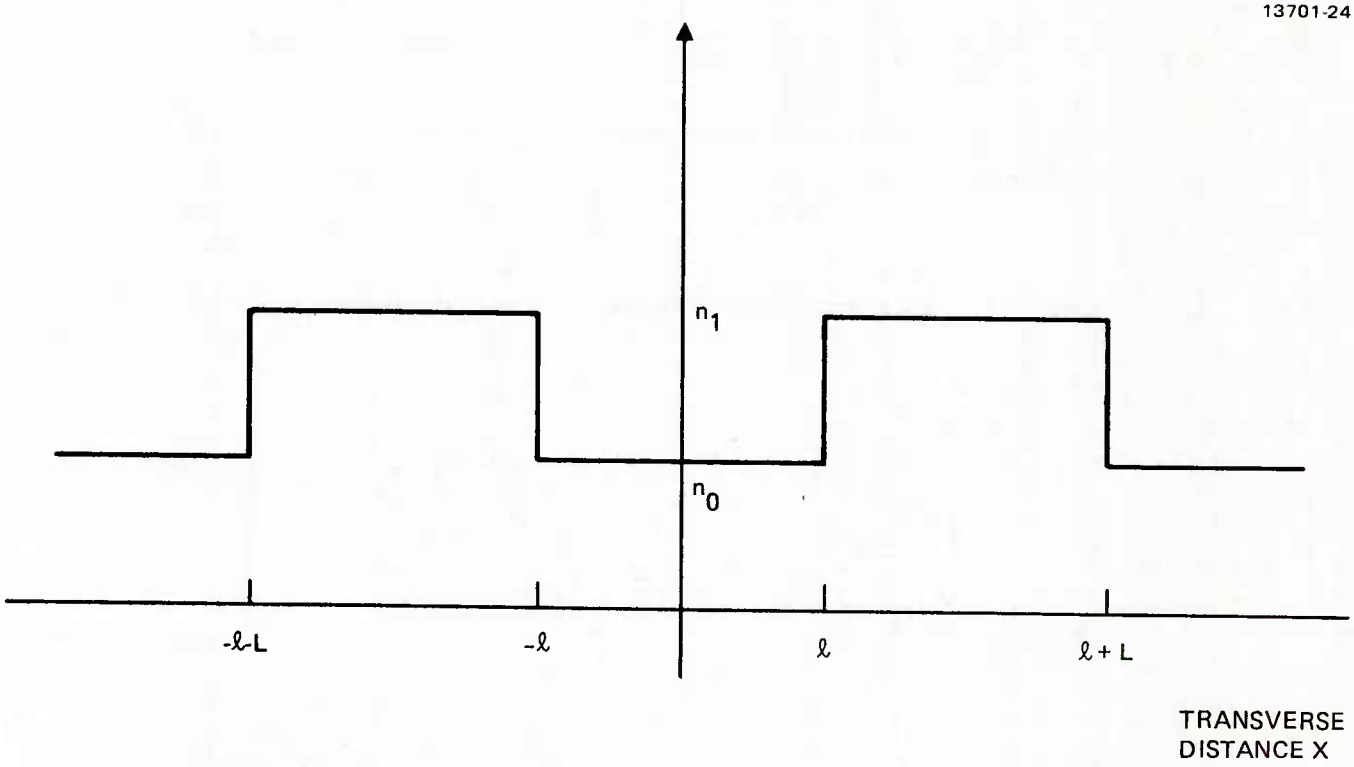

Figure 32. Relative size of the index of refraction as a function of the transverse dimension of the waveguide system.

$$u(x) = A\, a^{k_0 x}, \quad x < -\ell - L$$

$$u(x) = \begin{cases} B \cos k_1 x \\ \\ C \sin k_1 x \end{cases}, \quad -\ell - L < x < -\ell$$

$$u(x) = \begin{cases} D\, a^{k_0 x} \\ \\ E\, a^{-k_0 x} \end{cases}, \quad |x| < \ell \qquad (24)$$

$$u(x) = \begin{cases} F \cos k_1 x \\ \\ G \sin k_1 x \end{cases}, \quad \ell < x < \ell + L$$

$$u(x) = H\, a^{-k_0 x}, \quad x > \ell + L$$

The following dispersion relations are found in the same manner as before.

a) Even symmetric solutions, or odd antisymmetric solutions

$$\frac{\tan k_1 \ell}{\tan k_1 (\ell + L)} = = \tanh k_0 L \qquad (25)$$

b) Even antisymmetric solutions, or odd symmetric solution,

$$\frac{\tan k_1 \ell}{\tan k_1 (\ell + L)} = -\coth k_0 \ell \qquad (26)$$

Figure 33 shows a plot of the dispersion relation as a function of the product of β and the waveguide dimension L for the case of even-symmetric or odd-antisymmetric solutions. Figure 33 shows two curves which represent the right and left hand sides of Eq. (25). The intersection points are the allowed values of β for fixed lengths ℓ and L. For example, if $\beta L = 67.6$, one can count that there exist five allowed normal modes.

The next case to be considered is the triple planar waveguide system illustrated in Figures 34 and 35. Again the solutions can be written in a similar manner as before, and the application of boundary conditions yields the dispersion relations. For simplicity we shall consider the even-symmetric solutions. The dispersion relation is given by

$$\frac{k_0}{k_1} = \frac{\tan k_1 \left(2\ell + 3\frac{L}{2}\right)}{\tan k_1 \left(2\ell + \frac{L}{2}\right)} \frac{\tanh k_0 \left(2\ell + \frac{L}{2}\right)}{\tanh \frac{k_0 L}{2}} \tan \frac{k_1 L}{2} \qquad (27)$$

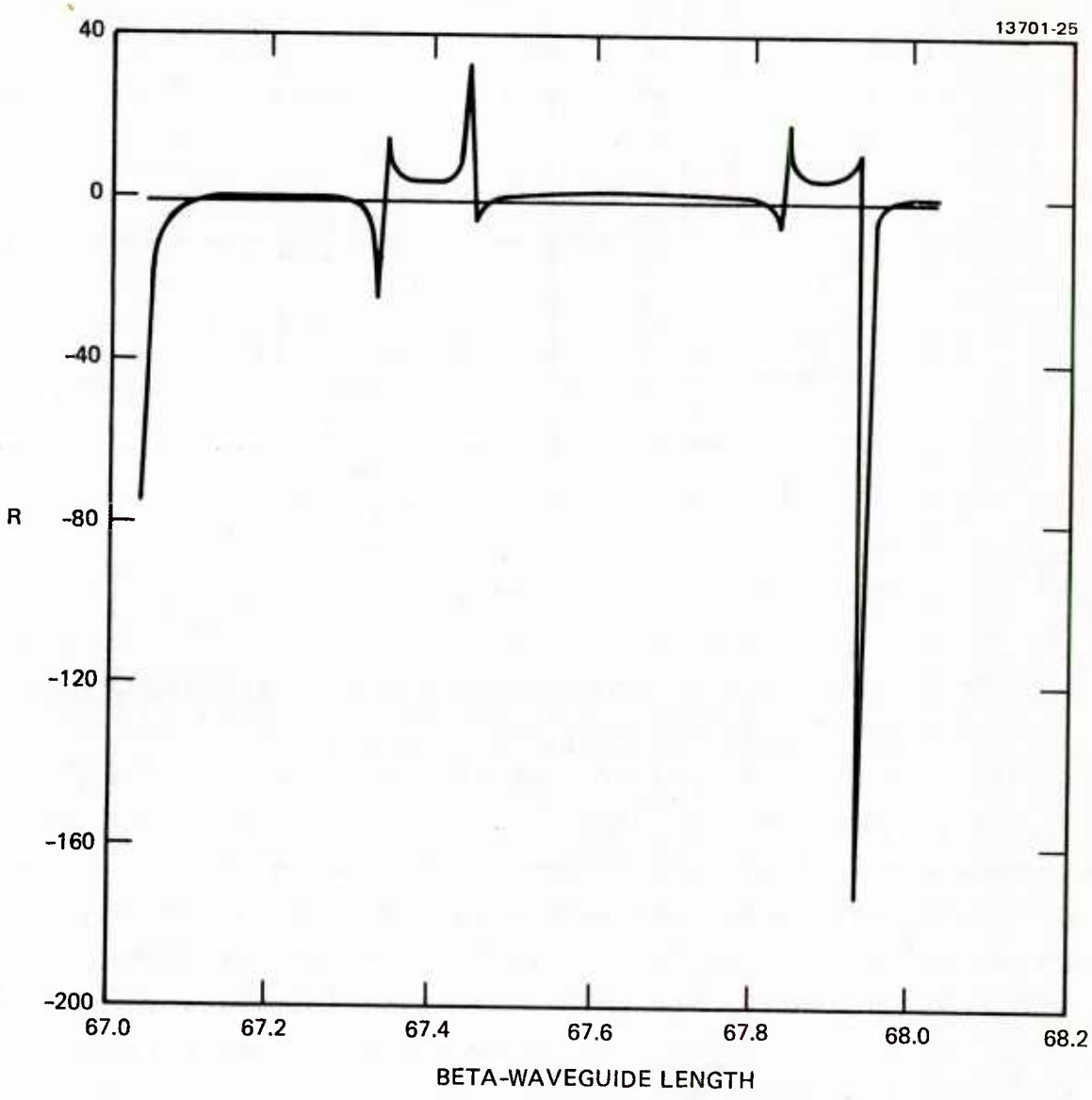

Figure 33. Dispersion relation for the even-symmetric or odd-antisymmetric solutions of the double planar waveguide system.

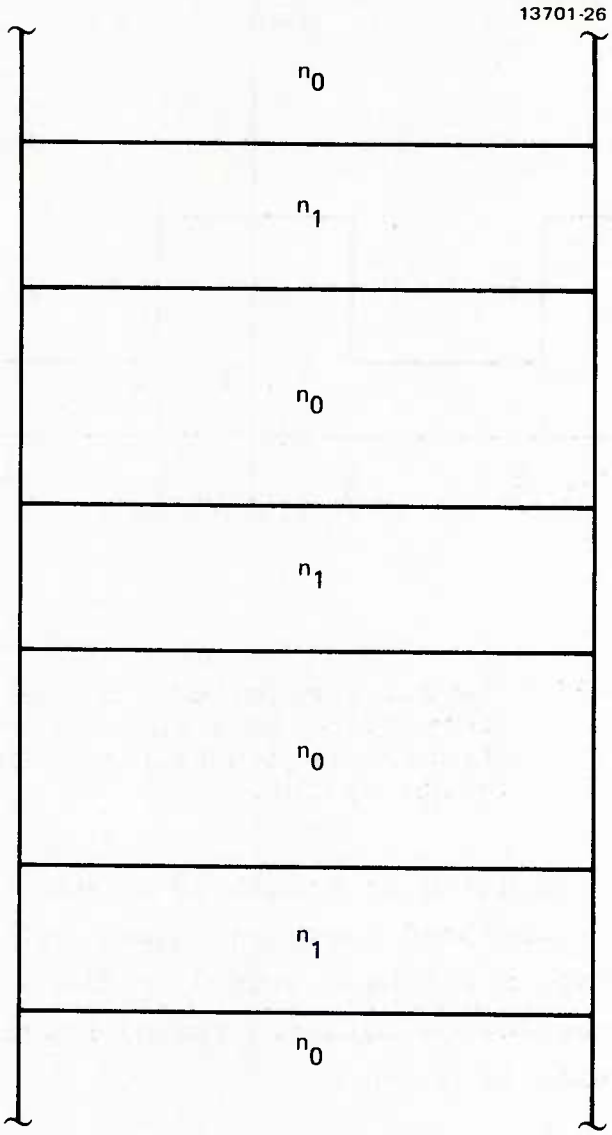

Figure 34. Geometry for the triple planar waveguide system.

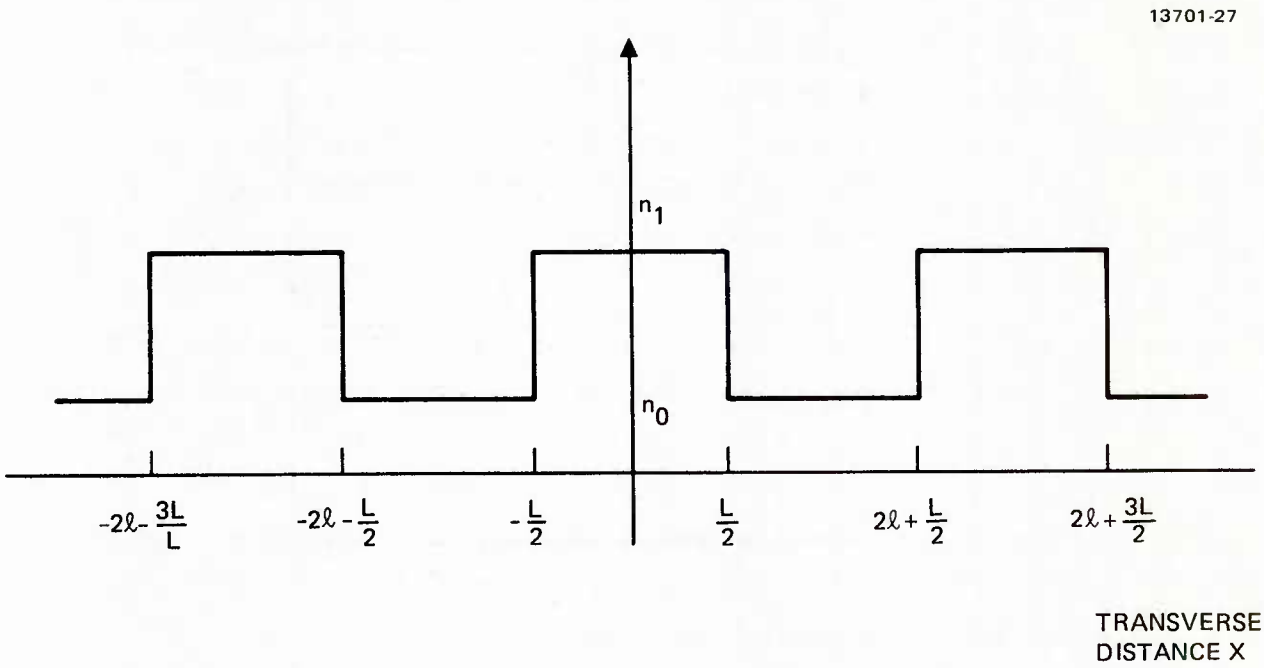

Figure 35. Relative magnitude of the indices of refraction as a function of the transverse dimension of the waveguide system.

Equation (27) is plotted in Figure 36 showing two curves corresponding to the right- and left-hand sides of the equation. Identical interpretation can be assigned to the significance of the crossing or intersection points. The dispersion for the even-antisymmetric mode is given by

$$\frac{k_0}{k_1} = \frac{\tan k_1 \left(2\ell + 3\frac{L}{2}\right)}{\tan k_1 \left(2\ell + \frac{L}{2}\right)} \frac{\coth k_0 \left(2\ell + \frac{L}{2}\right)}{\coth \frac{k_0 L}{2}} \tan \frac{k_1 L}{2} \qquad (28)$$

and a similar curve can be obtained from Eq. (28).

The double and triple planar waveguide systems form the basis for obtaining, by inspection, the mode structure of the 2N and 2N+1 planar waveguide systems, respectively. The conclusion

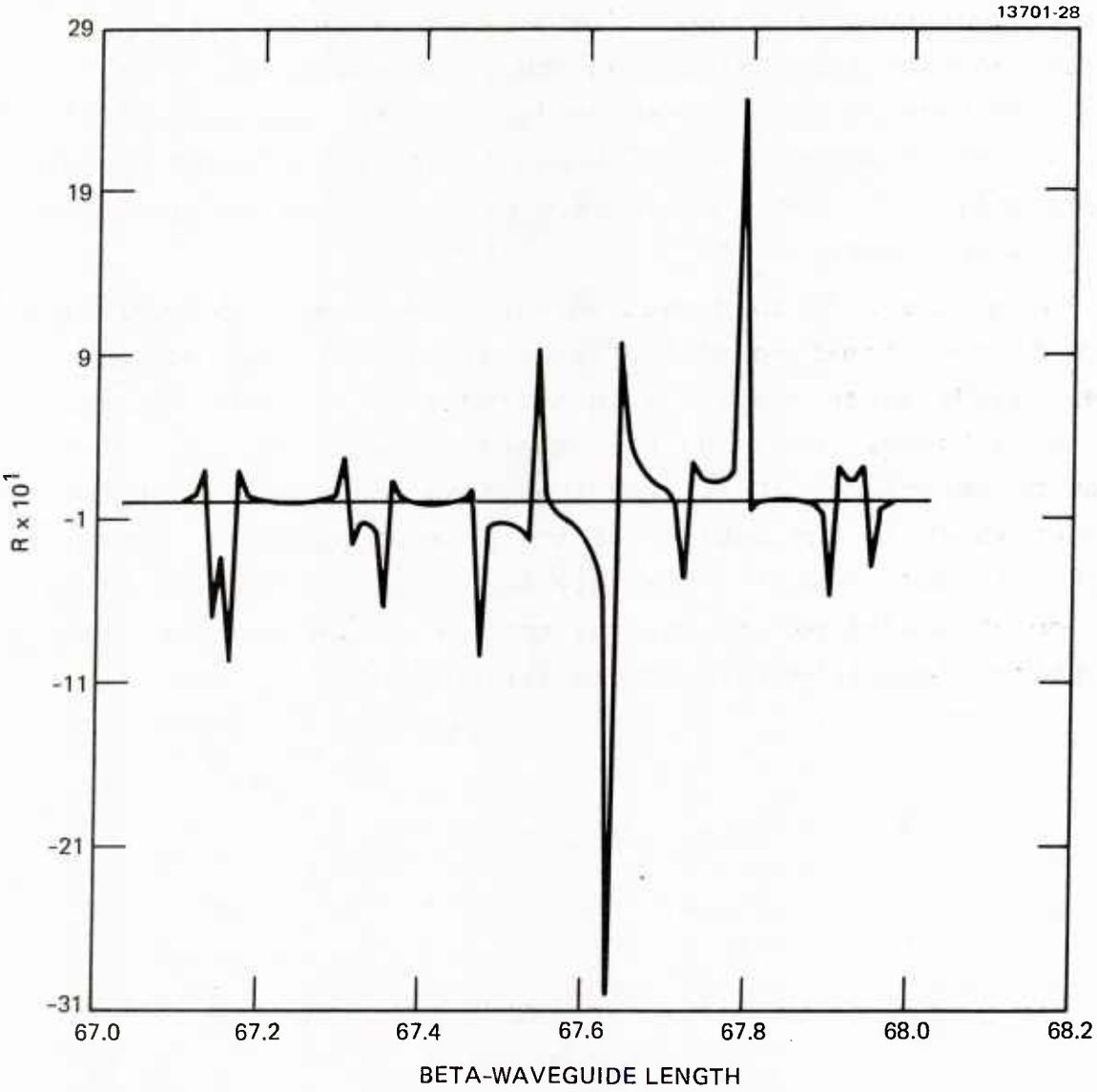

Figure 36. Dispersion relation for the case of even symmetric solutions in the triple planar waveguide system.

that we can draw is that there are intrinsically 4 types of normal modes; even symmetric and antisymmetric, and odd symmetric and antisymmetric. Any input field can then be expressed in terms of these modes. The analysis of the phased-array diode laser system can benefit from the knowledge that the output field is no more than the superposition of these modes with the appropriate coefficients. The coefficients are obtained from the gain equations for the laser oscillation.

The analysis of this section has been used to describe the nature of the normal modes that will arise in a coupled multi-element diode laser array. This analysis is relevant for many coupling schemes, including the evanescent-wave approach represented by References 10-12, and the phase-conjugate resonator approach which is the subject of the present program. These analytical results will ultimately be helpful in understanding which modes should be selected by some means in order to achieve the optimum far-field intensity distribution.

SECTION 3

CANDIDATE PHASE CONJUGATE MIRRORS

The use of a phase conjugate resonator to couple multiple diode gain elements was introduced in Section 1. In principle, aberrations arising from differences in the individual gain elements are automatically compensated by the phase conjugate mirror (PCM). This section considers what PCM concepts are compatible with the wavelength range and power levels of the multi-element GaAlAs diode laser. Specifically, we have considered phase conjugation by the process of stimulated Brillouin scattering (SBS). This approach avoids the requirement for external, high quality pump lasers necessary to construct a PCM based on four-wave mixing. However, because of the $\lesssim$ 1 GHz frequency shift imparted to the laser radiation as part of the SBS process, this approach can only be utilized in pulsed applications where the bandwidth of the gain medium is broad enough to accomodate the accumulated frequency shift. For a 4-nm bandwidth, a 10-cm-long resonator could operate at pulse lengths up to 1 μsec.

Stimulated Brillouin scattering is a threshold process: only if the incident light intensity exceeds a minimum value will appreciable reflection occur. Hence, a crucial condition is the threshold intensity for SBS to arise. The objective of this section is to calculate such a threshold intensity for two types of optical waveguides. One is filled with carbon disulfide (CS_2) and the other one is composed of fused quartz. The expression for the threshold intensity is given by[19]

$$I_{th} = \frac{16\ cT\ \epsilon_o^2\ n_1^2\ n_2}{\gamma^2\ k_1 k_s\ L_1 L_s} \tag{29}$$

where c is the velocity of light, T is the bulk modules, ϵ_o is the permeability of free space, n_1 and n_2 are the indices of refractior

at the pump and SBS frequencies, respectively, γ is the electrostriction coefficient, k_1 is the wavevector of the pump; k_2 is the wavevector of the acoustic wave, L_1 is the attenuation length of the pump and L_s is the attenuation length of the acoustic wave. For the case of CS_2, one finds that the threshold intensity is approximately given by

$$I_{th} = 0.75 \times 10^5 \frac{\text{watts}}{\text{cm}^2} \tag{30}$$

The threshold energy for SBS can then be calculated as

$$E_{th} = 0.75 \times 10^5 \frac{\text{watts}}{\text{cm}^2} \times \text{Area} \times \tau \tag{31}$$

where τ is the pulse duration, and the area is the input cross-section at the entrance of the multimode waveguide system. Figure 37 shows a plot of the threshold energy versus optical fiber diameter for distinct values of τ. The optical fiber is assumed to be filled with liquid CS_2. The wavelength chosen for this calculation is 700 nm. However, CS_2 has a large bandwidth for SBS and should be able to accommodate all GaAlAs diode laser wavelengths. In the case of SiO_2 optical fiber one finds that the threshold power is[20]

$$P_{th} = \frac{20\,A}{gL_{eff}} \tag{32}$$

where A is the cross section of the optical fiber, g is the SBS gain and L_{eff} is the damping length of the electromagnetic wave. Experimental measurements[20] yield $g = 4.3 \times 10^{-9}$ cm/Watt and $L_{eff} = 2 \times 10^4$ cm. The threshold energy is then

$$E_{th} = 1.72 \times 10^5 \times \text{Area} \times \tau \tag{33}$$

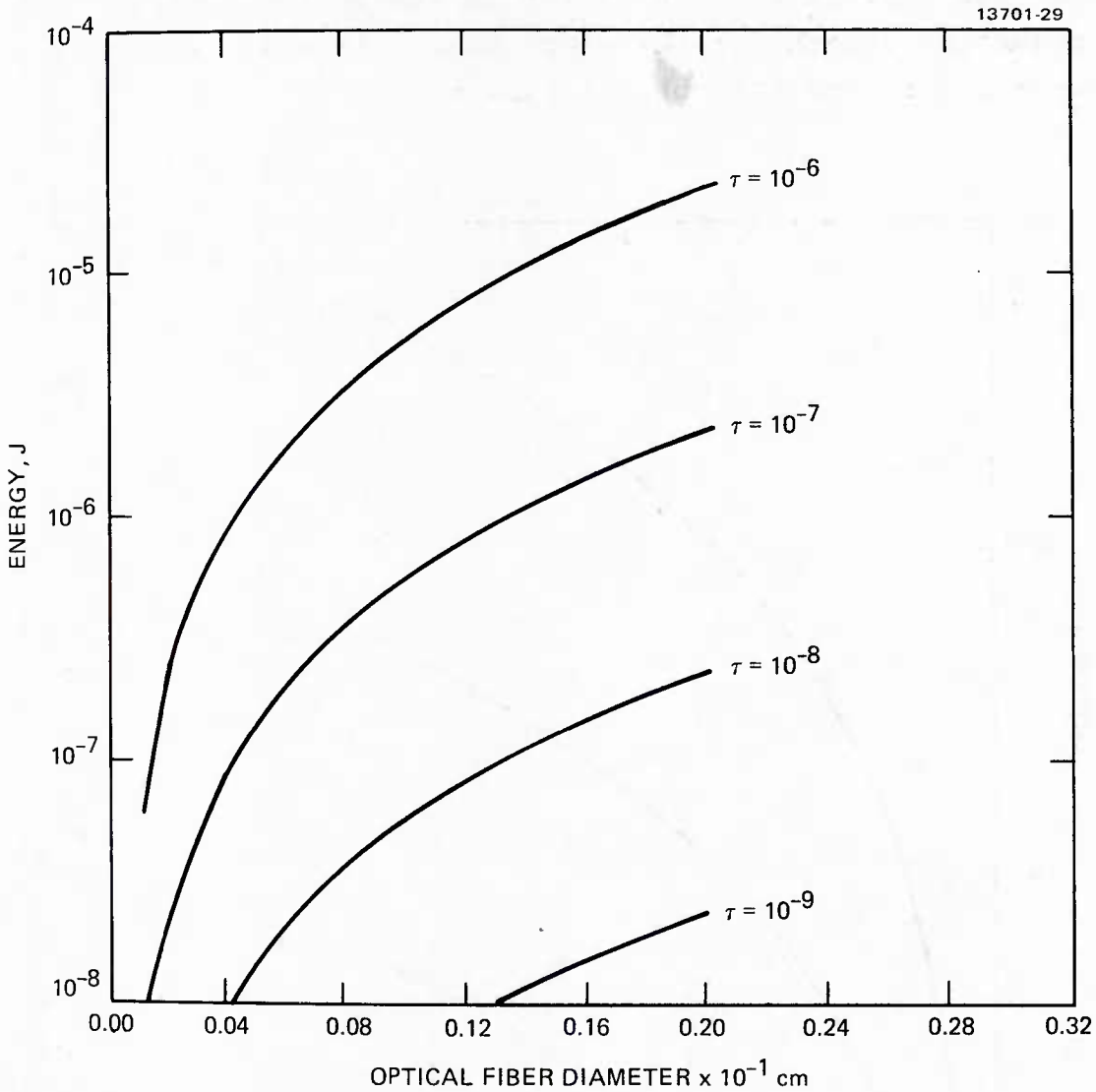

Figure 37. SBS threshold energy versus optical fiber diameter for several pulse lengths. The optical fiber is assumed to be filled with liquid CS_2.

Figure 38 shows a plot of E_{th} vs fiber diameter for the SiO_2 fiber. These results indicate that the threshold energy requirement for the generation of phase conjugate waves by SBS is rather low. The smallness of the value is due to two factors: long attenuation length for the electromagnetic wave, and small input cross-section for the optical fibers.

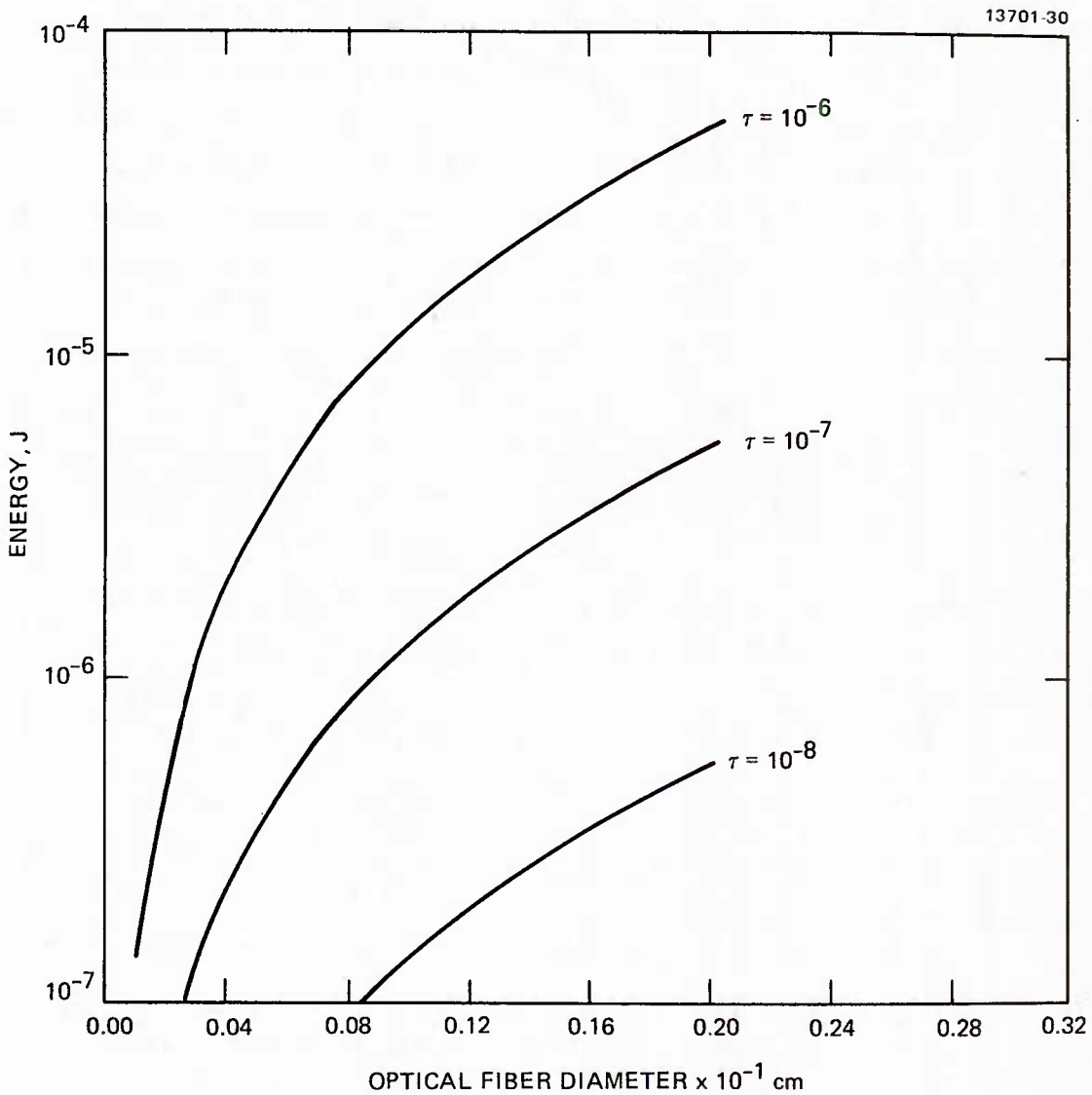

Figure 38. SBS threshold energy versus optical fiber diameter for several pulse lengths. The optical fiber is made of SiO_2.

SECTION 4

HIGH EFFICIENCY FREQUENCY DOUBLING CONCEPTS

4.1 INTRODUCTION

In this section we show that, if concepts for the co-phasing of diode gain media can be successfully implemented, then frequency doubling with efficiencies consistent with the requirements of practical military applications appear possible. This calculation is based on published results[21] describing the successful (but low efficiency <0.2 percent) demonstration of frequency doubling using the crystal $KNbO_3$, driven by a GaAlAs diode laser operating at 860 nm. By scaling these results and using the high peak power and narrow linewidth properties anticipated from the proposed diode phased arrays, it appears that as few as thirteen commercial diode lasers operating coherently will provide sufficient peak power to achieve 40 percent doubling efficiency. In addition, the following analysis indicates that high efficiency will be achievable at kilowatt power levels, providing the doubling process can be scaled without sacrificing efficiency. Hughes feels this can be accomplished with a minimum number of nonlinear crystals based on considerable experimental and theoretical research on the problems involved in scaling frequency doubling devices to high average power.

In this section we first lay the groundwork for predicting efficiency using well established principles. These principles are then used to select a doubling crystal, where we find that $KNbO_3$ is the best candidate for the present application, although other materials are also identified. We then describe the scaling concepts which lead to the high efficiency (40 percent) doubling potential. A discussion of the solutions to frequency-doubler scaling problems is then presented.

4.2 NONLINEAR CRYSTAL SELECTION

This section reviews the physical principles that ensure efficient frequency doubling in the absence of the severe thermal effects that arise in scaling to high average power. (Power scaling is discussed in Section 4.4). Consideration of these principles leads to a set of selection criteria for a nonlinear crystal appropriate for the present application. Several crystal candidates are described. In the following section one material is selected and baseline performance is predicted using this material.

Frequency doubling has been studied for twenty years; the basic analytical equations describing the process are readily available,[22] and show that the doubling efficiency for a fundamental wave at a frequency ω with its power P_1 uniformly distributed over an area A is given by

$$\eta = 2 \left(\frac{\mu_o}{\varepsilon_o}\right)^{3/2} \frac{\omega^2 d^2 L^2}{n^3} \left[\frac{\sin(\Delta kL/2)}{\Delta kL/2}\right]^2 \frac{P_1}{A} \qquad (34)$$

where d is the appropriate nonlinear coefficient for a crystal with an interaction length L and refractive index n, and

$$\Delta k = k_2 - 2k_1 \qquad (35)$$

is the difference between the second-harmonic wavevector k_2 and twice the fundamental wavevector k_1. Equation (34), which neglects depletion of the fundamental beam, shows that doubling efficiency is maximized by selecting a material with a high nonlinear coefficient, a long interaction length, and by arranging for phase matching to occur ($\Delta k = 0$). Phase matching occurs when the fundamental and second-harmonic beams propagate through the crystal with the same phase velocity.

The technique to achieve phase matching utilizes the natural birefringence of anisotropic crystals. With a suitable choice of the polarization and the propagation direction of the fundamental wave, there often exists a different polarization for the second harmonic that allows propagation at the same phase velocity as the fundamental. When considering practical applications in which high doubling efficiency is imperative, however, this "critical" phase matching is undesirable for two reasons. First, as the extraordinary wave propagates through the crystal, its direction of power flow differs from the direction of its wavevector.[23] This leads to a gradual walk-off of the extraordinary wave from the ordinary wave, and severely limits the effective interaction length of the nonlinear crystal.[24] Second, the required angular tolerance on the propagation direction of the fundamental can typically be as small as 1 mrad for a 1 cm interaction length, thereby limiting the allowed beam divergence of the fundamental wave.

For these two reasons, it is preferred to utilize crystals that allow non-critical, 90 degree phase matching.[25] In this configuration, the beams propagate along a crystal axis. Consequently the walk-off does not occur, and the angular tolerance is greater by typically an order of magnitude. Often, noncritical phase matching may be achieved by adjusting the crystal temperature until the refractive indices reach appropriate values. Unfortunately, this is not always possible if the refractive indices are not sufficiently temperature dependent, or if the necessary phase matching temperature lies outside practical limits. For example, temperatures $\lesssim 0°C$ are inconvenient because of potential window frost problems, or the required temperature might be near a phase transition or crystal degradation temperature.

Additional factors affecting crystal selection include optical quality and uniformity, transparency at both the fundamental and second harmonic wavelengths, resistance to surface,

bulk, and index damage, availability and damage resistance of antireflection coatings, and various physical properties such as crystal stability and hygroscopicity.

Such considerations lead to the selection of $KNbO_3$ as the optimum crystal for doubling GaAlAs radiation.[21] Promising alternatives include $KTiOPO_4$ (KTP), recently the subject of significant developmental effort supported by the Air Force, $Ba_2NaNb_5O_{15}$, and $LiNbO_3$.

4.3 FREQUENCY DOUBLER DESIGN

In the work described in Reference 21, radiation from a diode laser having 0.196 W of peak power lying within the 0.09 nm phase matching bandwidth was focused into the $KNbO_3$ crystal. The observed second harmonic power of 0.34 mW (doubling efficiency of 0.18 percent) is slightly more than that expected from Eq. (34). In an earlier article,[26] the same author reported a conversion efficiency of 15 percent using a higher power parametric oscillator source at the same 860 nm wavelength, but having a narrower linewidth of 0.045 nm. Those experimental results are shown in Figure 39. Once again, the result was in good agreement with the predictions of Eq. (34). It is important to note that no saturation effects for the doubling efficiency were evident for fundamental intensities up to 0.5 MW/cm^2, the maximum available from that pump laser, indicating that greater efficiency is expected for higher intensities.

The implications of this previous work on the present study are significant in that they show that $KNbO_3$ can be non-critically phase matched to produce second-harmonic wavelengths between 430 nm and 470 nm, with longer wavelengths possible by raising the crystal temperature. In addition, the crystal behavior was close to that expected from theoretical calculations. It is appropriate, therefore, to use those results in estimating performance of such a frequency doubler when used with a high power

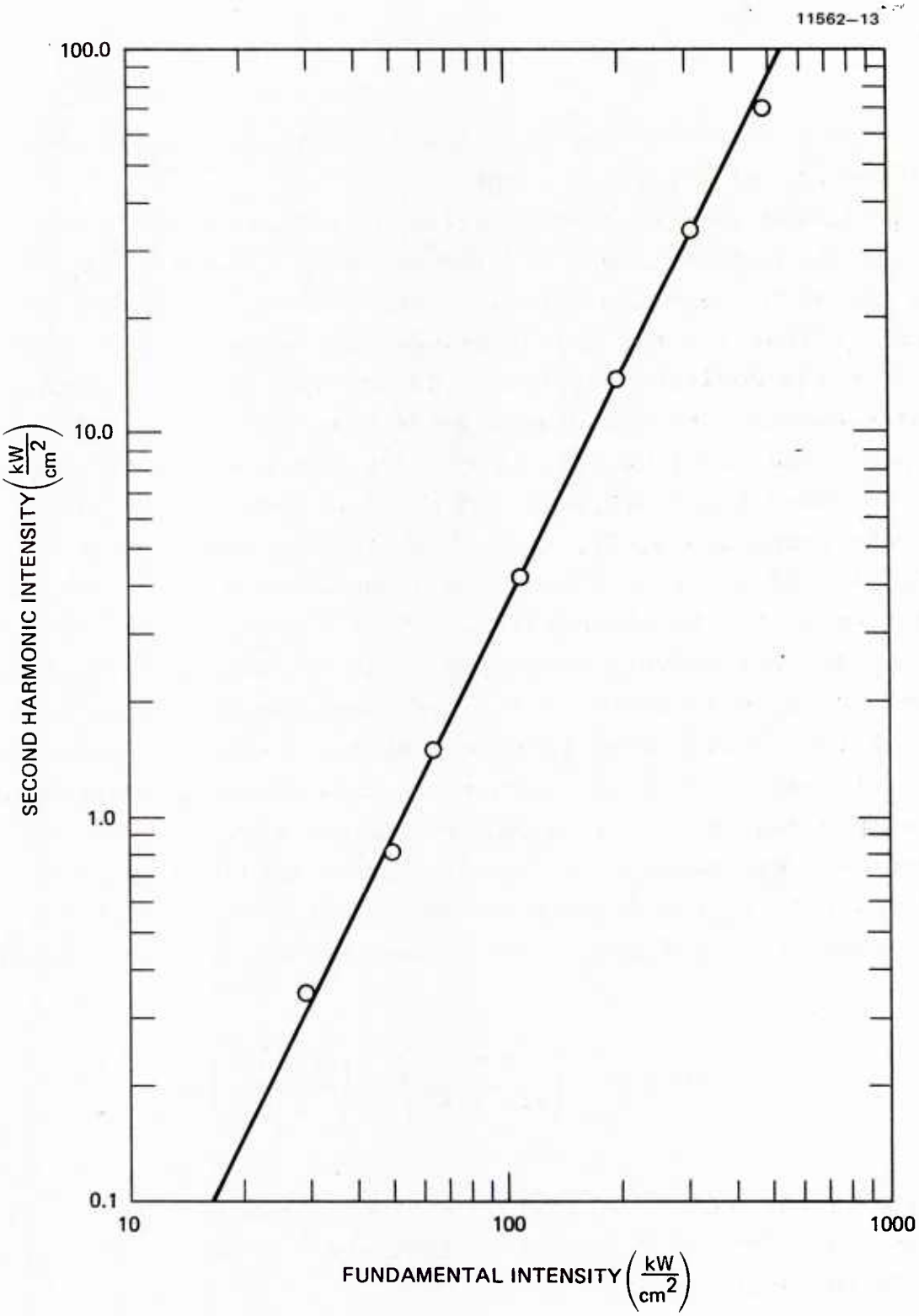

Figure 39. Second harmonic power density as a function of fundamental power density for non-critically phase matched second harmonic generation at room temperature in $KNbO_3$. Crystal length is 5.74 mm. (From Reference 26).

diode laser source as an indicator of what is expected when scaling to large phased arrays of diodes.

The experimental configuration of Reference 21 incorporated optical elements to focus the radiation of a single GaAlAs laser into the $KNbO_3$ doubling crystal. The optical design was selcted to ensure that all the radiation was just within the acceptance angle of the nonlinear crystal. In scaling up to the number of diode elements, and consequently the beam dimensions, to increase the power and doubling efficiency, the focal length of the lens used to focus the radiation into the nonlinear crystal must increase proportionately, i.e., the f-number must remain constant, in order not to exceed the acceptance angle. Under this condition it can be shown that if the diode radiation distributions are effectively compacted in such a way as to minimize "dead" areas (see Section 2.3), the intensity of the central lobe of the focused beam increases linearly with the number of diode elements. This is most easily understood by considering the simple case of linear array of N plane wave sources of dimension s separated by a distance d. Diffraction theory[27] predicts that in the focal plane of a lens with a focal length f the intensity at a distance x off the optical axis is given by

$$I(x) = \frac{sP}{f\lambda} \left(\frac{\sin \frac{Nkdx}{2f}}{\sin \frac{kdx}{2f}} \right)^2 \left(\frac{\sin \frac{ksx}{2f}}{\frac{ksx}{2f}} \right) \qquad (36)$$

where P is the power radiated by a single source, λ is the wavelength, and $k = 2\pi/\lambda$. Consider first the case where $N = 1$; the on-axis intensity is

$$I_1(0) = \frac{sP}{f_1\lambda} \qquad (37)$$

and f_1 is determined by the acceptance angle of the nonlinear crystal. The on-axis intensity for the case of N sources adding coherently is

$$I_N(0) = \frac{sP}{f_N \lambda} N^2 \tag{38}$$

where f_N is the array focal length. In order to maintain constant f-number, one requires that

$$\frac{f_N}{Nd} = \frac{f_1}{s} \tag{39}$$

Equation (38), then becomes

$$I_N(0) = N\left(\frac{s}{d}\right)\left(\frac{sP}{f_1 \lambda}\right) = N \frac{s}{d} I_1(0) \tag{40}$$

When s/d approaches unity, we find $I_N(0) \approx N I_1(0)$. One of the requirements for the multi-element diode laser is to develop phased array designs in which s/d may indeed approach unity (see the discussion in Section 2.3).

Having established this simple relationship, it is possible to use the scaling results of Figure 39 to calculate how many commercially available diodes are required to increase the peak intensity from 3.9 kW/cm^2 in Reference 21 to 1 MW/cm^2, thereby increasing the doubling efficiency from 0.15 percent to 40 percent, a practical value typical of present hardware. The output characteristics of the diode used in Reference 21 are shown in Table I, along with those of representative commercial diodes. Even allowing for transmission losses of as much as 20 percent in the beam shaping optics, it is clear that approximately 20 times more power is available, within a narrower

Table I. Diode Laser Output Characteristics

Type	Unspecified	RCA SG2012	Laser Diode LD-67
Wavelength, nm	860.0	904.0	904.0
Bandwidth, nm	1.2	3.5	3.5
Half-Angle Beam Spread -			
Parallel to Junction, deg	10.0	7.5	7.0
Normal to Junction, deg	18.0	9.0	10.0
Peak Power, watt	0.78[a]	20.0[b]	20.0[b]
Pulse Length, nsec	10.0	200.0	200.0
Duty Cycle, Percent	-	0.1	0.1
Reference	21	28	29

[a]Power focused into nonlinear crystal

[b]Minimum total peak power

divergence angle, than was used in Reference 21. Thirteen of these higher power diodes would produce 260 W peak power (with s/d = 1). With the same f-number as Reference 21 (i.e., a focal length of ∿1 m) the required peak intensity of 1 MW/cm^2 could be generated.

In summary, phase matching requirements lead to the selection of $KNbO_3$ as the best nonlinear crystal. Using established doubling performance data, a peak intensity of 1 MW/cm^2 is projected to produce a practical 40 percent doubling efficiency. The required peak intensity can be provided by the coherent operation of only thirteen commercial diode lasers.

Greater doubling efficiency may be achieved using intracavity doubling. However, to predict performance of that configuration, more detailed knowledge is required concerning such parameters as single-pass gain and output coupling.

4.4 FREQUENCY DOUBLER SCALING ISSUES

Historically, the design of high average power frequency doubled systems has been difficult because of the lack of a full understanding and appreciation of the physical mechanisms and phenomena operating in the nonlinear crystal during high power operation. This has been aggravated by a paucity of reliable data on the crystal properties, particularly radiative absorption, that parameterize the power scaling relationships. The absorption measurement is difficult because the small absorptions involved cannot be measured by conventional photometric methods; also, nonlinear absorption effects sometime arise. Compounding these difficulties is the variability in crystal properties with vendor.

The difficulties that have been encountered in frequency doubling technology may be divided into four broad areas:

1. Efficiency of the doubling process and how it is limited by crystal type and uniformity, crystal environment, and laser beam properties.

2. Measurement of the crystal properties, most importantly absorption, that parameterize high power operation. Absorption in the crystal is the origin of the thermal effects that limit output power.

3. Understanding the thermal effects. This includes both transient and steady-state effects. Absorption induces temperature gradients in the crystal and the oven housing it. Gradients outside the beam interaction region cause transient effects and instabilities in the temperature control. Gradients in the interaction region degrade doubling efficiency as they disrupt the phase match conditions. They also cause birefringence in the crystal.

4. Damage and deterioration mechanisms of the materials involved. For lower average power operation, surface and bulk damage from high peak power must be considered. At high average power, crystal fracture resulting from thermal stress or shock must also be eliminated. For long life, material sensitivity to environmental factors must be understood and controlled.

Each of these difficulties has been addressed by Hughes in earlier frequency doubler designs. The important results are summarized here for each issue:

1. Non-critically phase matched (90 degree phase matched) materials have a great advantage over angle phase matched in that they do not impose stringent beam divergence or alignment requirements on the pump laser source for high efficiency. Higher doubling efficiencies are also obtainable.

2. Several parameters are important for quantifying frequency doubler power handling. Absorption is certainly the most important. Sensitive calorimetric methods must be utilized for measuring the small absorptions involved, so that average power limits of materials can be modelled.

3. Thermal effects in the crystals are the primary cause of instability and limit the power handling. Transient problems can be overcome by proper crystal oven design and the use of electro-optic tuning[30] (EOT) which provides fast response to perturbations and always maintains the oven at the correct temperature. Also, beam shaping[31] has been shown to eliminate the average power limit and fracture problems caused by temperature gradients in the interaction region.

4. Damage has been found to be a limiting factor in many frequency doubling systems. Many such problems are eliminated by careful control of contaminants, particularly in the crystal oven where outgassing aggravates the problem. In addition, conservative design guidelines on acceptable flux levels have been developed using empirical data.

Because of their essential role in the high average power frequency doubler design, the techniques of beam shaping and electro-optic tuning will be discussed briefly.

4.4.1 Beam Shaping

The maximum output power of any frequency-doubling crystal is ultimately determined by the temperature gradients arising from radiative absorption in the crystal. This limit manifests itself in two ways. First, because the crystal refractive indices are, in general, temperature dependent it is impossible to maintain phase matching across the entire beam profile in the presence of severe temperature gradients. Second, with a conventional focusing geometry which produces a circular laser spot on the nonlinear crystal, thermally induced stresses arise which are essentially symmetric about the laser axis. These stresses depolarize the radiation passing through the nonlinear crystal; the depolarized component is no longer phase matched and is effectively removed from the doubling process.

The solution to this problem is called beam shaping: cylindrical lenses shape the pump beam into an ellipse on the face of the nonlinear crystal. A careful, but straightforward thermal analysis[31] of this configuration indicates that the maximum temperature difference across the laser profile is reduced by the factor (h/w) relative to that for a circular spot, where h and w are the height and width of the laser spot, respectively. For example, simply reducing h and increasing w each by a factor of four would keep the illuminated area and the intensity constant, but would reduce the temperature difference and increase the maximum output power by a factor of sixteen relative to that for a circular spot (h/w = 1). In addition, to the extent that heat

flow in the crystal is one-dimensional (using a low, wide crystal geometry slightly larger than h and w assures this), a judicious choice of pump beam polarization either a parallel or perpendicular to the direction of heat flow eliminates the depolarization problem when 90° phase matching is used.

4.4.2 Electro-Optic Tuning

Electro-optic tuning[30] (EOT) is a technique to provide transient control of frequency doubling. It is useful when long warmup periods are undesirable, or when a high degree of output amplitude stability is required. EOT is based on the fact that the refractive indices of a nonlinear crystal, and thus the phase match condition, may be controlled much more rapidly by changing the voltage across the crystal than by changing its temperature. In operation, it is initially assumed that the crystal is near, but not necessarily exactly at, the optimum phase match temperature. A voltage of plus (minus) ΔV is applied to the crystal for all the odd (even) pulses. Using a photodiode to measure the second harmonic output energy, simple electronic logic rapidly adjusts the average crystal voltage V_o until all output pulses are of equal energy, an indication that optimum phase matching has been achieved at the peak of the doubling efficiency versus temperature or voltage curve. Longer term logic changes the oven temperature in such a direction that V_o never exceeds a few kilovolts. EOT can correct for temperature excursions as much as a few degrees Kelvin.

SECTION 5

CONCLUSIONS

This research program was aimed at investigating several technical areas related to scaling the output power of diode lasers by coherent coupling techniques. We have seen that the far-field intensity distribution of a linear array of phase-locked diode lasers is highly sensitive to the number spacing and relative phase shift of adjacent emitters. Comparison with recently published experimental results indicates that a phase shift of 180° occurs most often, producing a slightly undesirable two-lobed far-field pattern. Computer simulations of locking multiple diode elements in a phase conjugate resonator show that no such problem arises in this case, and that the output beam quality is determined solely by the quality of the resonator output mirror. This positive result is the motivation for considering such a coupling scheme. Further computer simulations including practical features such as waveguiding effects are recommended as a point of further study. While such calculations were beyond the scope of the present program, a first step was undertaken in calculating the lowest order normal modes of a multiple-element planar waveguide. We have also considered the deleterious effects on beam quality of relatively large gaps between emitters (to accomodate cooling, for example), and have proposed several beam compacting schemes to minimize these effects. The proposed schemes are considerably more practical in a phase conjugate resonantor than they would be using other coupling schemes (e.g., evanescent-wave coupling).

The phase conjugate mirror involved in constructing a phase conjugate resonator always involves some trade-offs. While devices based on degenerate four-wave mixing (DFWM) are conceptually quite simple, operate at very low powers, and are available over a wide spectral range, their use in the present application is somewhat undesirable because of a practical reason:

the pump lasers required to operate the DFWM phase conjugate mirror must be diffraction-limited beams with a total power close to that of the multiple-diode phase conjugate resonator. In other words, the pump laser must be essentially the same as the laser we are trying to construct. This recognition leads one to consider alternative phase conjugation techniques; specifically, stimulated Brillouin scattering (SBS). While SBS does not require any external pump laser, it does impart a small frequency shift ($\lesssim$ 1 GHz) on the reflected beam. Hence, SBS would be most practical in pulsed applications in which the accumulated frequency shift could be less than the ~ 4 nm laser gain bandwidth (a 10-cm long resonator could accomodate pulses of at least 1 μsec duration). We have analyzed two representative SBS media for potential application to a diode-based phase conjugate resonator: a fused silica fiber, and a CS_2-filled light guide. In either case, we find threshold intensities of ~ 10^{-4} - 10^{-5} w/cm^2, values which could likely be achieved with a high power diode array. This fact supports the feasibility of a diode-based phase conjugate resonator.

We have also considered the practical issues involved in achieving efficient frequency doubling with a high power diode laser. Non-critically phase-matched materials are preferred because of their wide angular tolerance and long interaction lengths. The baseline material selected is $KNbO_3$; based on published data on the doubling efficiency of this material, we find that 13 coherently coupled commercial diode lasers could provide sufficient brightness to achieve 40% extracavity doubling efficiency. Hence, wavelength conversion of a high power diode laser array also seems practical.

The conclusion is that the basic concept of coupling multiple diode lasers in a phase conjugate resonator appears feasible. Further theoretical studies would be appropriate before attempting an experimental demonstation. These studies should include waveguiding effects, as well as realistic performance

modeling for the phase conjugate mirror. The analysis presented in the body of this report shows that sufficient brightness can be obtained to allow efficient wavelength conversion by nonlinear processes. Using demonstrated frequency doubler power scaling techniques, an efficient, high power diode-based source could produce radiation in the blue-green spectral region for a variety of applications.

REFERENCES

1. J. AuYeung, D. Fekete, D.M. Pepper, and A. Yariv, IEEE J. Quantum Electron. QE-15, 1180 (1979).

2. J.M. Bel'dyugin, M.G. Galushkin, and E.M. Zemskov, Sov. J. Quantum Electron. 9, 20 (1979).

3. J.F. Lam and W.P. Brown, Opt. Lett. 5, 61 (1980).

4. P.A. Belanger, A. Hardy, and A.E. Siegman, Appl. Opt. 19, 602 (1980).

5. E.M. Phillipp-Rutz, Appl. Phys. Lett. 26, 475 (1975).

6. R.H. Rediker, Progress Report for period 1 July 1980 - 30 June 1981 "Fiber Coupled External Cavity Semiconductor Laser," Sept. 10, 1981 MIT.

7. H.W. Yen, Hughes Research Laboratories, private communication.

8. J. Zorootchi and J.K. Butler, J. Appl. Phys. 44, 3697 (1973).

9. C. Slayman, Hughes Research Laboratories, private communication.

10. D.R. Scifres, R.D. Burnham, C. Lindstrom, W. Streifer, and T.L. Paoli, Appl. Phys. Lett. 42, 645 (1983), and references therein.

11. D.E. Ackley, Appl. Phys. Lett. 42, 152 (1983).

12. J. Katz, S. Margalet, and A. Yariv, Appl. Phys. Lett. 42, 554 (1983).

13. J. Goodman, Introduction to Fourier Optics (New York, McGraw-Hill, 1968).

14. D.R. Scifres, R.D. Burnham, and W. Streifer, Appl. Phys. Lett. 41, 118 (1982).

15. A.E. Siegman, P.A. Belanger and A. Hardy, "Optical Resonators Using Phase Conjugate Mirrors," in Optical Phase Conjugation ed. by R.A. Fisher, (Academic Press, New York, 1982), Chapter 10.

16. G. Harburn, C.A. Taylor, and T.R. Welberry, Atlas of Optical Transforms, (Cornell University Press, Ithaca, NY, 1975).

17. G.P. Agrawal and M. Lai, J. Opt. Soc. Am. 69, 1717 (1979).

18. D. Marcuse, Theory of Dielectric Optical Waveguides (New York, Academic, 1974).

19. A Yariv, Quantum Electronics (New York, Wiley, 1975).

20. E. Ippen and R. Stoler, Appl. Phys. Lett. 21, 539 (1972).

21. P. Gunter, P.W. Asbeck, and S.K. Kurtz, Appl. Phys. Lett 35, 461 (1979).

22. Amnon Yariv, Introduction to Optical Electronics (Holt, Rinehart and Winston, New York, 1971), pp. 189-194.

23. Max Born and Emil Wolf, Principles of Optics (Pergamon, New York, 1975), p. 668.

24. G.D. Boyd, A. Ashkin, J.M. Dziedzic, and D.A. Kleinman, Phys. Rev. 137, A1305 (1965).

25. Frits Zernike and John E. Midwinter, Applied Nonlinear Optics (Wiley, New York, 1973), p. 68.

26. P. Gunter, Appl. Phys. Lett. 34, 650 (1979).

27. Max Born and Emil Wolf, ibid, p. 405.

28. "Single-Diode Injection Lasers," RCA data sheet for SG2000, SG2000A Series, 1977.

29. "Single Heterojunction GaAs Laser Diodes, LD60 Series," Laser Diode Laboratories, Inc., data sheet.

30. David T. Hon, IEEE J. Quant. Electron. QE-12, 148 (1976), and J. Appl. Phys. 49, 396 (1978).

31. David T. Hon and H. Bruesselbach, IEEE J. Quant. Electron, QE-16, 1356 (1980).

DISTRIBUTION LIST

REPORT NO. Final Report, N00014-82-C-0535

Agency	No. of Copies
Director Defense Advanced Research Projects Agency Attn: Technical Library 1400 Wilson Blvd. Arlington, Virginia 22209	3
Office of Naval Research Physics Division Office (Code 412) Attn: H.S. Pilloff 800 North Quincy Street Arlington, Virginia 22217	4
Office of Naval Research Director, Technology (Code 200) 800 North Quincy Street Arlington, Virginia 22217	1
Naval Research Laboratory Department of the Navy Attn: Technical Library Washington, DC 20375	3
Office of the Director of Defense Research and Engineering Information Office Library Branch The Pentagon Washington, DC 20301	3
U.S. Army Research Office Box 1211 Research Triangle Park North Carolina 27709	2
Defense Technical Information Center Cameron Station Alexandria, Virginia 22314	12
Director, National Bureau of Standards Attn: Technical Library Washington, DC 20234	1
Commanding Officer Office of Naval Research Western Detachment Office 1030 East Green Street Pasadena, California 91101	3
Commanding Officer Office of Naval Research Eastern/Central Detachment Office 495 Summer Street Boston, Massachusetts 02210	3

Director
U.S. Army Engineering Research
and Development Laboratories
Attn: Technical Documents Center
Fort Belvoir, Virginia 22060 — 1

ODDR&E Advisory Group on Electron Devices
201 Varick Street
New York, New York 10014 — 3

Air Force Office of Scientific Research
Department of the Air Force
Bolling AFB, DC 22209 — 1

Air Force Weapons Laboratory
Technical Library
Kirtland Air Force Base
Albuquerque, New Mexico 87117 — 1

Air Force Avionics Laboratory
Air Force Systems Command
Technical Library
Wright-Patterson Air Force Base
Dayton, Ohio 45433 — 1

Lawrence Livermore Laboratory
Attn: Dr. W. F. Krupke
University of California
P.O. Box 808
Livermore, California 94550 — 1

Harry Diamond Laboratories
Technical Library
2800 Powder Mill Road
Adelphi, Maryland 20783 — 1

Naval Air Development Center
Attn: Technical Library
Johnsville
Warminster, Pennsylvania 18974 — 1

Naval Weapons Center
Technical Library (Code 753)
China Lake, California 93555 — 1

Naval Training Equipment Center
Technical Library
Orlando, Florida 32813 — 1

Naval Underwater Systems Center
Technical Center
New London, Connecticut 06320 — 1

Commandant of the Marine Corps
Scientific Advisor (Code RD-1)
Washington, DC 20380 — 1

Naval Ordnance Station
Technical Library
Indian Head, Maryland 20640 — 1

Naval Postgraduate School
Technical Library (Code 0212)
Monterey, California 93940 — 1

Naval Missile Center
Technical Library (Code 5632.2)
Point Mugu, California 93010 — 1

Naval Ordnance Station
Technical Library
Louisville, Kentucky 40214 — 1

Commanding Officer
Naval Ocean Research & Development Activity
Technical Library
NSTL Station, Mississippi 39529 — 1

Naval Explosive Ordnance Disposal Facility
Technical Library
Indian Head, Maryland 20640 — 1

Naval Ocean Systems Center
Technical Library
San Diego, California 92152 — 1

Naval Surface Weapons Center
Technical Library
Silver Spring, Maryland 20910 — 1

Naval Ship Research and Development Center
Central Library (Code L42 and L43)
Bethesda, Maryland 20084 — 1

Naval Avionics Facility
Technical Library
Indianapolis, Indiana 46218 — 1